AD-769 963

THIN FILM OPTICAL WAVEGUIDES IN III-V SEMICONDUCTORS

M. George Craford

Monsanto Company

Prepared for:

Air Force Cambridge Research Laboratories
Defense Advanced Research Projects Agency

July 1973

ARPA Order No. 2074

Program Code No. 3D10

Contractor: Monsanto Co.

Effective Date of Contract: 1 July 1972

Contract No. F19628-72-C-0324

Principal Investigator & Phone No.
Dr. M. George Craford/314 694-3647

AFCRL Project Scientist & Phone No.
Dr. Andrew C. Yang/617 861-2225

Contract Expiration Date:
31 December 1973

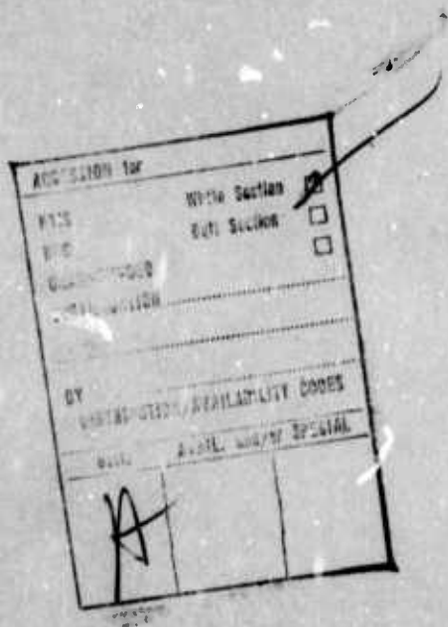

Qualified requestors may obtain additional copies from the Defense Documentation Center. All others should apply to the National Technical Information Service.

ib

Unclassified
Security Classification

AD. 769963

DOCUMENT CONTROL DATA - R&D

(Security classification of title, body of abstract and indexing annotation must be entered when the overall report is classified)

1. ORIGINATING ACTIVITY *(Corporate author)*
Monsanto Company/Electronic Products Division
800 N. Lindbergh Boulevard
St. Louis, Missouri 63166

2a. REPORT SECURITY CLASSIFICATION
Unclassified

2b. GROUP

3. REPORT TITLE

THIN FILM OPTICAL WAVEGUIDES IN III-V SEMICONDUCTORS

4. DESCRIPTIVE NOTES *(Type of report and inclusive dates)*
Scientific. Interim.

5. AUTHOR(S) *(First name, middle initial, last name)*

M. George Craford

6. REPORT DATE
July 1973

7a. TOTAL NO. OF PAGES
83

7b. NO. OF REFS
8

8a. CONTRACT OR GRANT NO. ARPA Order No. 2074
F19628-72-C-0324

b. PROJECT, TASK, WORK UNIT NOS.
2074 n/a n/a

c. DOD ELEMENT 61101E

d. DOD SUBELEMENT n/a

9a. ORIGINATOR'S REPORT NUMBER(S)
Semi-Annual Technical Report No.2

9b. OTHER REPORT NO(S) *(Any other numbers that may be assigned this report)*
AFCRL-TR-73-0533

10. DISTRIBUTION STATEMENT

A - Approved for public release; distribution unlimited.

11. SUPPLEMENTARY NOTES
This research was supported by the Defense Advanced Research Projects Agency.

12. SPONSORING MILITARY ACTIVITY
Air Force Cambridge Research Laboratories (LQ)
L. G. Hanscom Field
Bedford, Massachusetts 01730

13. ABSTRACT

The development of techniques for the growth of large area vapor phase epitaxial GaAs and GaAsP, and liquid phase epitaxial GaAs and GaAlAs, waveguide structures is described. GaAs n/n+ and GaAs/GaAsP waveguide structures have been grown and evaluated and the results have been compared to calculated attenuation rates. The results demonstrate the advantages of an alloy structure for GaAs waveguides at 10.6μm wavelength. An analysis of waveguides with graded indices of refraction is described. A preliminary demonstration of Bragg's diffraction Electro-optical Modulation in GaAs waveguides has also been obtained.

i

DD FORM 1 NOV 65 1473

Unclassified
Security Classification

14. KEY WORDS	LINK A		LINK B		LINK C	
	ROLE	WT	ROLE	WT	ROLE	WT
Gallium arsenide						
Gallium arsenide phosphide						
Gallium aluminum arsenide						
Vapor phase epitaxy						
Liquid phase epitaxy						
Integrated optics						
Thin film waveguides						
Electro-optical modulation						
Optical attenuation						

AFCRL-TR-73-0533

THIN FILM OPTICAL WAVEGUIDES IN III-V SEMICONDUCTORS

by

M. George Craford

Monsanto Company
Electronic Products Division
800 N. Lindbergh Boulevard
St. Louis, Missouri 63166

Contract No. F19628-72-C-0324
Project No. 2074

Semi-Annual Technical Report No. 2

July 1973

Contract Monitor: Andrew C. Yang
Solid State Sciences Laboratory

Sponsored by
Defense Advanced Research Projects Agency
ARPA Order No. 2074

Monitored by

AIR FORCE CAMBRIDGE RESEARCH LABORATORIES
AIR FORCE SYSTEMS COMMAND
UNITED STATES AIR FORCE
BEDFORD, MASSACHUSETTS 01730

iC

ABSTRACT

The development of techniques for the growth of large area vapor phase epitaxial GaAs and GaAsP, and liquid phase epitaxial GaAs and GaAlAs, waveguide structures is described. GaAs n/n+ and GaAs/GaAsP waveguide structures have been grown and evaluated and the results have been compared to calculated attenuation rates. The results demonstrate the advantages of an alloy structure for GaAs waveguides at 10.6 μm wavelength. An analysis of waveguides with graded indices of refraction is described. A preliminary demonstration of Bragg's diffraction Electro-optical Modulation in GaAs waveguides has also been obtained.

FOREWORD

This semi-annual technical report covers the work performed under contract F19628-72-C-0324 between the period December 31, 1972 to July 1, 1973.

The objective of this program is to grow a variety of epitaxial GaAs, GaAsP and GaAlAs waveguide structures and to evaluate their performance with regard to the propagation of 10.6 μm radiation. The effect of such parameters as layer thickness, alloy composition profile, and carrier concentration will be investigated. Vapor phase epitaxial techniques will be employed to grow the GaAsP structures and liquid phase epitaxial techniques to grow the GaAlAs structures.

Technical direction is being provided by Dr. Andrew Yang of the Air Force Cambridge Research Laboratory. The growth of the epitaxial structures is being carried out in the Monsanto Commercial Products Company, Electronic Products Division, Laboratories, St. Louis, Missouri, and the waveguide evaluation has been subcontracted to and is being performed in the laboratories of the Washington University School of Engineering and Applied Science, St. Louis, Missouri.

The research carried out on this program is under the direction of M. George Craford. Others directly involved in this work and in the preparation of this report are D. Finn, W. O. Groves, and A. H. Herzong. of Monsanto Company, and W. S. C. Chang, M. Muller, and H. R. Vann, of Washington University.

TABLE OF CONTENTS

TABLE OF CONTENTS (Continued)

LIST OF FIGURES

LIST OF TABLES

SECTION I

SUMMARY OF RESULTS

The results of the activities during the first six months are summarized as follows:

A. VAPOR PHASE EPITAXY (VPE)

A modified growth technique has been developed which produces GaAs films with carrier concentrations in the 1-5 x $10^{14}/cm^3$ range and with high mobilities.

A variety of GaAs n/n+ and GaAs/GaAsP structures have been submitted for evaluation. However, further work is required in order to reproducibly grow GaAs/GaAsP structures with good surface quality.

Efforts to develop a reproducible technique technique for the growth of high resistivity VPE epitaxial films ($\rho \gtrsim 10^6$ Ω-cm) have not yet been successful.

B. LIQUID PHASE EPITAXY (LPE)

A series of large area GaAlAs samples, up to two inches in length, have been grown which have good thickness and compositional uniformity. Several samples are now ready for the growth of a VPE epitaxial GaAs layer to complete the GaAs/GaAlAs waveguide structure.

C. WAVEGUIDE EVALUATION

Attenuation rate data collected on GaAs n/n+ and GaAs/GaAsP waveguide structures demonstrated the advantages of the alloy structures for GaAs waveguides at 10.6 μm wavelength.

A preliminary demonstration of Bragg's diffraction Electro-Optical Modulation in GaAs waveguides has been obtained.

An analysis of waveguides with graded indices of refraction has been completed.

Work on two dimensional waveguides has been initiated.

SECTION II

VAPOR PHASE EPITAXY

A. INTRODUCTION

The objectives of the Vapor Phase Epitaxy (VPE) portion of this program are to grow various n/n+ GaAs, $GaAs/GaAs_xP_{1-x}$, $GaAs_xP_{1-x}/GaAs/GaAs_xP_{1-x}$ and $GaAs/Ga_xAl_{1-x}As$ structures to determine the effect of various parameters including film thickness, carrier concentration and alloy composition on waveguide properties at 10.6 μm. Structures of the first two types have been grown during the second portion of this program.

B. RESULTS OBTAINED IN PRODUCTION SCALE VPE REACTORS

During the second quarter silicon was identified by emission mass spectrophotometer analysis as the principal background impurity in growing undoped GaAs films using the Group V hydride feed system and the HCl transport of the gallium. Typical carrier levels for 25 μm thick films grown at normal operating conditions varied from 1-3 x $10^{16}/cm^3$ as shown in Table I. Thick films of 75 μm or greater showed net carrier concentrations in the low $10^{15}/cm^3$ range. The reduction in carriers in the thicker films is produced by the gettering properties of the GaAs predeposit which forms on the quartz reactor above the substrate holder. The thick films thus contain a carrier gradient. The effect of the predeposit on reducing the background doping level is clearly seen from the data in Table II in which a dummy run (without substrate) of 30-60 minutes was made to partially coat the reactor wall. Substrates were then loaded into the reactor and a deposit of 25 μm was made at the same growth conditions given in Table I. The carrier level was reduced by approximately an order of magnitude.

A carrier concentration profile of run 220 as determined by step etching and capacitance-voltage measurements is shown in Figure 1. These data show a relatively constant carrier level throughout the sample except for about a 2 μm region adjacent to the substrate epitaxial interface. The higher doping in this region is believed to be the result of autodoping from the substrate.

The production of silicon contamination in the reactor is believed to result from reactions of hydrogen and/or hydrogen chloride (HCl) with the quartz reactor. Products of these reactions include various chlorosilanes, silion chlorides, silicon monoxide

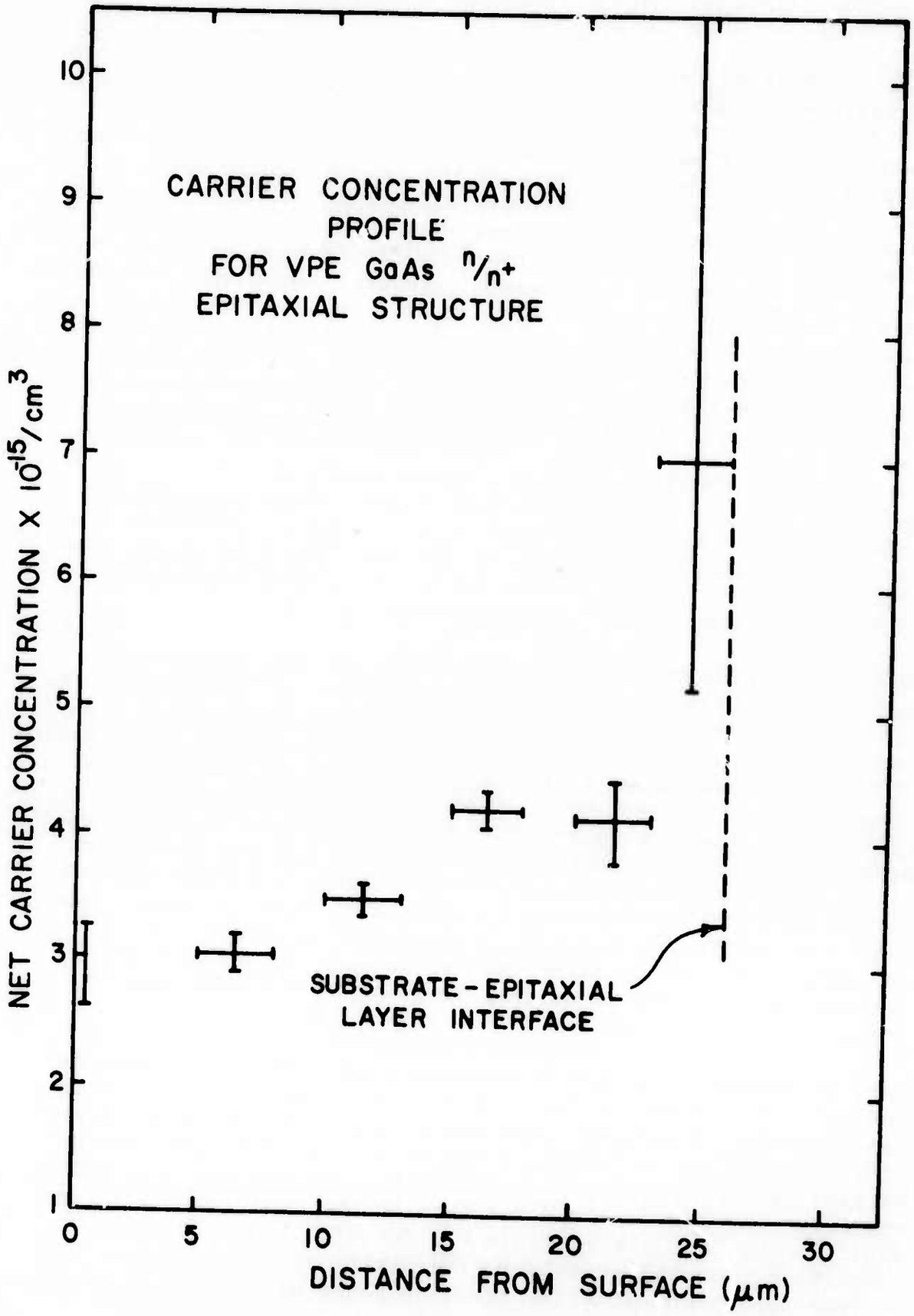
CARRIER CONCENTRATION
PROFILE
FOR VPE GaAs n/n+
EPITAXIAL STRUCTURE
NET CARRIER CONCENTRATION X 10^15/cm^3
DISTANCE FROM SURFACE (μm)
SUBSTRATE-EPITAXIAL
LAYER INTERFACE
0
5
10
15
20
25
30
1
2
3
4
5
6
7
8
9
10

Figure 1

(SiO), and water vapor. Since the reactions are partially reversible the addition of water to the reactor should suppress the formation of silicon compounds and thus reduce the carrier level of undoped material. Several experiments were performed in an effort to identify areas of the reactor where most of the silicon is generated by feeding a 300 ppm H_2O/H_2 mixture to the various reactor feed inlets. The results of these data are summarized in Table III. In the runs in which water was added to the two main hydrogen streams there were reductions of approximately 50 percent in the background silicon level with a water concentration of 60 ppm based on total reactor feed. However, with an overall water concentration of less than 4 ppm when added to the HCl/H_2 feed to the gallium source the background carrier level was reduced to roughly 30 percent of the normal undoped level (see Table I). These experiments agree quantitatively with Monsanto Company results obtained with the gallium phosphide (GaP) system several years ago. They apparently indicate that the major portion of the silicon impurities found at those operating conditions are derived from HCl-quartz reactions. Attempts to modify the reactor design to reduce the background doping level have been unsuccessful.

Previous studies on GaP have shown that the net carriers in nitrogen doped layers were lower by a factor of 2-3 than in the non-nitrogen doped film. This suggested the possibility that ammonia (NH_3) may reduce the silicon level in GaAs. The addition of NH_3 in concentrations of 3-8 mole percent of the feed gas lowered the background level of undoped GaAs films to 2-3 x $10^{15}/cm^3$ as shown in Table III. It is important to note that the room temperature mobility of these samples are low indicating either appreciably compensation and/or heavy nitrogen addition to the crystal. Preliminary evaluation of these nitrogen doped layers by Washington University showed an unusually high absorption for the measured carrier level. Because of this problem and the lack of success in lowering the carriers, further investigations with NH_3 additions were discontinued.

Results obtained previously using gallium/arsenic trichloride ($AsCl_3$) feed system and small horizontal reactors for growing GaAs indicate that background levels may be drastically lowered by the proper set of growth parameters. (1) The application of similar techniques to the production reactor has resulted in approximately a fifty-fold decrease in the background level as indicated by the data in Table V. The high liquid nitrogen mobility of run 287 attests to the purity of the material. The surface appearance of films grown at these conditions is marginal,

i.e., they contain some irregular shaped pits which are believed to be caused by particulate matter falling on the wafers during growth.

Part of the contract calls for the growth of a double layered structure; the first layer being a low doped GaAsP alloy deposit of 20 microns or greater followed by a low doped GaAs ($10^{15}/cm^3$) layer of 5-30 μm of GaAs. Preliminary attempts to grow 36% phosphorous alloys with carriers less than $10^{15}/cm^3$ were not successful because of surface imperfections and high carriers ($\times 1 \times 10^{16}/cm^3$). This approach was temporarily discontinued in hopes that some heterostructures could be more quickly grown using off-specification red LED material as substrate for the GaAs films. The growth of films on alloy substrates was characterized by an enhancement of the cross-hatch which results from grading the alloy composition. This effect is clearly shown in Figure 2. Removing the cross-hatch by mechanically polishing the alloy substrates did not reduce the problem. Modifications in the start-up of the GaAs growth cycle alleviated the enhancement of the cross-hatch but introduced pits (See Figure 3) and increased the net electrical carriers of the GaAs film to the low $10^{15}/cm^3$ range. Various modifications of the growth process -- particularly start-up conditions -- have been tried, and a number of waveguide structures have been evaluated, but the results have been erratic. There are apparently other undefined factors such as possibly strain in the crystal or point defects which have large effects on the surface morphology and doping characteristics.

In the future the GaAs/GaAsP heterostructures will be produced by growing the entire structure continuously in the same reactor. This process should result in a reduced number of interfacial defects and will, hopefully, overcome some of the problems encountered using the two step technique described here.

Figure 2

GaAs/GaAsP Sample Showing Pronounced Cross-Hatch Effect

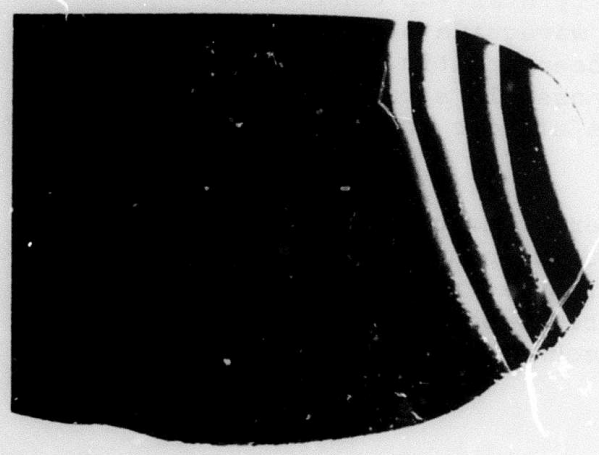

Figure 3

GaAs/GaAsP With Reduced Cross-Hatch Effect, But With Increased Pit Density

TABLE I

Background Silicon Contamination Level at Normal Operating Conditions

Run No.	Deposition Temp, C	Net Carriers η, cm^{-3}	Mobility @300K cm^2/volt-sec	Film Thickness, μm
206	748	1.7×10^{16}	6230	28
208	746	2.1×10^{16}	5230	28
209	743	2.2×10^{16}	5190	29
211	749	1.8×10^{16}	5130	30

TABLE I

Background Silicon Contamination Level at Normal Operating Conditions

Run No.	Deposition Temp, C	Net Carriers η, cm^{-3}	Mobility @300K cm^2/volt-sec	Film Thickness, μm
206	748	1.7×10^{16}	6230	28
208	746	2.1×10^{16}	5230	28
209	743	2.2×10^{16}	5190	29
211	749	1.8×10^{16}	5130	30

TABLE II

Effect of Predeposit on the Background Contamination Level*

Run No.	Deposition Temp, C	Net Carriers η, cm^{-3}	Mobility @300K cm^2/volt-sec	Film Thickness, μm
212	747	2.3×10^{15}	7510	29
213	752	2.9×10^{15}	7040	23
220	749	3.0×10^{15}	7150	26
228	744	2.2×10^{15}	7180	25
229	763	2.6×10^{15}	6610	25

* Reactor coated for 30-60 min before deposition.

TABLE III

Effect of Water Addition on the Background Contamination Level

Run No.	Deposition Temp, C	H_2O Feed Point	H_2O/H_2* Feed, sccm	Overall H_2O Conc. in Reactor	Net Carriers n, cm^{-3}
233	755	Flush H_2 Group III Side	400	30 ppm	1.0×10^{16}
234	762	Main H_2 Group V Side	800	60 ppm	8.4×10^{15}
236	755	H_2/HCl Feed to Ga	50	3.8	6.4×10^{15}
237	759	H_2/GCl Feed to Ga	50	3.8	5.8×10^{15}

* 300 ppm H_2O/H_2 mixture.

TABLE IV

Effect of the Addition of NH_3 on the Background Silicon Level in Undoped GaAs

Run No.	Deposition Temp, C	NH_3 Feed Conc. Mole %	Net Carriers η, cm^{-3}	Mobility @300K cm^2/ volt-sec
241	762	8.5	1.7×10^{15}	5540
244	763	5.0	3.2×10^{15}	5180
245	761	2.5	2.7×10^{15}	5220

Film Thickness = 25-30 μm

TABLE V

Undoped Epitaxial GaAs Grown
at Modified $Ga/AsCl_3$ Growth Conditions

Run No.	Deposition Temp, C	Net Carriers η, cm^{-3}	Mobility @300K μ, cm^2/volt-sec	Film Thickness μm
278	745	8.5×10^{14}	7800	12.7
279	749	4.2×10^{14}	7860	9.8
280	745	7.5×10^{14}	7600	21.5
287	730	1.4×10^{14}	8340	8.8
289	736	3.0×10^{14}	8110	13.8

Run 287 Electricals @77K

$\eta = 1.59 \times 10^{14}/cm^3$

$\mu = 92{,}330\ cm^2$ volt-sec

C. RESULTS OBTAINED ON THE GROWTH OF HIGH RESISTIVITY GaAs IN RESEARCH SCALE VPE REACTORS

As reported in the previous Semi-Annual Technical Report, techniques for producing high resistivity VPE GaAs layers have been explored mainly using laboratory scale horizontal reactors in order to minimize developmental costs. The high resistivity epitaxial layers are required for d.c. modulation techniques applied to GaAs waveguides. The results of these experiments will be summarized here although none of the approaches achieved reproducible growth of compensated high resistivity GaAs films. Two avenues were explored, compensated deep donor (Zn-O) doping, and deep acceptor (Cr or Fe) doping.

An apparently successful initial attempt at Zn-O doping, reported in the January Semi-Annual report, now appears due to an i-layer formed during the transition from Zn-O doping, probably p-type, to Te doping of the n-type surface contact layer. The major difficulties in growing individual high resistivity layers of Zn-O doped GaAs appear to be low O concentrations in spite of water vapor concentrations in the reactant gas as high as 0.67%, combined with strong dependence of Zn concentration or deposition temperature and poor control of the Zn dopout concentration at the very low flows required. As a result, the grown layers have been of low resistivity, either n- or p-type layers were produced simultaneously.

Control of zinc doping is complicated by zinc contamination of the system which can carry over to a subsequent run and by preconditioning of the system required before low zinc doping levels can be achieved. Both effects are probably due to decomposition and/or absorption of diethyl zinc in the line entering the reactor.

An increase in background donor concentration with increasing doping water vapor concentration may have been caused by sulfur contamination of the deionized water. Addition of Hg_2Cl_2 to the water, which should remove H_2S did sharply reduce the background donor concentration.

GaAs layers doped with Zn-O, but remaining n-type have shown lowering of mobilities at both 300K and 77K and from 25% to 50% freeze out of carriers between 300K and 77K. However, the data show poor correlation with zinc and oxygen doping concentration.

Doping with Cr to produce high resistivity VPE layers has not proved successful. It may be concluded that Cr is either not transported or not incorporated in sufficient concentration to affect the electrical properties. In addition, impurities in the Cr source can interfere with the desired electrical properties.

With the chromium source located in a small boat in the hottest zone of the furnace upstream of the substrates, one sample of Cr metal (Ventron) yielded conductive p-type layers, another (Atomergics) yielded compensated n-type layers. $CrCl_2$ produced high resistivity layers, but of poor surface quality due to etching by the HCl produced by reacting with H_2. An undoped run, after removal of the Ventron Cr from the system, also produced p-type layers, presumably due to Cu contamination. Emission spectroscoper analysis showed the Ventron Cr to contain 3-5 times more Cu than the Atomergics sample.

Both Cr metal (Atomergics) and $CrCl_2$, prereduced, when used in a reactor in which the source was located in the GaCl-H_2 stream out of contact with arsenic or deposited GaAs, yielded compensated n-type layers. However, on removal of the $CrCl_2$ source, subsequent runs produced $\sim 5 \times 10^{13}$ p-type material. Evidently the $CrCl_2$ introduces an n-type impurity as well as Cu which persists as a low level contaminant in the system.

Attempts to produce high resistivity VPE GaAs by iron doping have also been unsuccessful, again due to probable copper contamination. The carriers in four successive runs using the same source (Ventron iron wire) changed progressively from 6.4×10^{15} n-type to 1.5×10^{14} p-type. Better control of iron volatilization (Fe reacted with GaCl to form a Ga-Fe alloy) and a higher purity source are indicated. However, since previous reports [2] of Fe doping in GaAs have indicated maximum resistivities of only $<10^5$ ohm-cm for both VPE and bulk GaAs, these efforts were discontinued.

The apparent ease with which relatively uncompensated material of either p-type or n-type can be produced suggests a very low concentration of deep level impurities in these epitaxial layers. If a low concentration p-type background can be established, low level doping with oxygen may be the best route to high resistivity GaAs.

D. WAVEGUIDE STRUCTURES SUBMITTED FOR EVALUATION

The GaAs n/n+ and the GaAs/GaAsP waveguide structures which have been submitted for evaluation to Washington University during the past six months are summarized in Table VI and Table VII respectively. The tables show the submission date and the properties of the epitaxial structures as well as evaluation remarks for the samples. The evaluation of the samples is described more completely in SECTION IV.

TABLE VI

GaAs n/n+ Structures Submitted for Evaluation

Date	Film Thickness μm	Film Carrier Conc. lcc	Substrate Carrier Conc. lcc	Sample Number	Evaluation Remarks
1/ 8/73	26	$2.7x10^{15}$	$2.4x10^{18}$	VR5 231 (3-01)	m=0,1,2,3 1.2DB/cm,3.4,8.2,20
1/ 8/73	26	$2.7x10^{15}$	$2 \ x10^{17}$	VR5 231 (3-02)	erratic output coupling. Used 2-D waveguide exp.
1/ 8/73	26	$2.7x10^{15}$	$6 \ x10^{17}$	VR5 231 (3-03)	erratic output coupling. Used 2-D waveguide exp.
1/ 8/73	26	$2.7x10^{15}$	$1.1x10^{18}$	VR5 231 (3-04)	erratic measurements
2/ 5/73	34.3	$6.3x10^{14}$	$4 \ x10^{18}$	Bushan (4-01)	m=0,1,2,3,4 2.6DB/cm,4.7,7.4,10.7,18
2/ 5/73	34.3	$6.3x10^{14}$	$4 \ x10^{18}$	Bushan (4-02)	2-D waveguide exp.
2/ 5/73	34.3	$6.3x10^{14}$	$4 \ x10^{18}$	K.W. (4-03)	2-D waveguide exp.
2/19/73	29.4	$1.2x10^{15}$	$2 \ x10^{17}$	1-16 (5-01)	2-D waveguide exp.
2/19/73	29.4	$1.2x10^{15}$	$2 \ x10^{17}$	1-16 (5-02)	2-D waveguide exp.
2/19/73	29.4	$1.2x10^{15}$	$2 \ x10^{17}$	1-16 (5-03)	2-D waveguide exp.
2/19/73	29.4	$1.2x10^{15}$	$2 \ x10^{17}$	1-16 (5-04)	Unused too small for attn. meas.
2/19/73	29.4	$1.2x10^{15}$	$2 \ x10^{17}$	1-16 (5-05)	2-D waveguide exp.
2/19/73	29.4	$1.2x10^{15}$	$2 \ x10^{17}$	1-16 (5-06)	2-D waveguide exp.
2/19/73	23.4	$6.4x10^{14}$	$4 \ x10^{18}$	1-17 (6-01)	Modulation exp.
2/19/73	(39.2) t	$6.4x10^{14}$	$4 \ x10^{18}$	1-17 (6-02)	m=0 2.6 DB/cm
2/19/73	found to	$6.4x10^{14}$	$4 \ x10^{18}$	1-17 (6-03)	K.W.
2/19/73	be 23.4	$6.4x10^{14}$	$4 \ x10^{18}$	1-17 (6-04)	Modulation exp.
2/19/73	rather	$6.4x10^{14}$	$4 \ x10^{18}$	1-17 (6-05)	Modulation exp.
	than 39.2				

Continued

TABLE VI (CONTINUED)

Date	Film Thickness μm	Film Carrier Conc. lcc	Substrate Carrier Conc. lcc	Sample Number	Evaluation Remarks
3/19/73	17.6	3.9×10^{14}	4×10^{18}	VR5 282 (9-01)	poor surface m=0 6.6 DB/cm
3/19/73	17.6	3.9×10^{14}	2×10^{18}	VR5 282 (9-02)	too small for attn. meas.
3/19/73	17.6	3.9×10^{14}	2×10^{18}	VR5 282 (9-03)	too small for attn. meas.
3/28/73	13.8	3.0×10^{14}	1×10^{18}	VR5 289 (10-01)	Good 2-D waveguide 13DB/cm ≈35μm wide
3/28/73	13.8	3.0×10^{14}	1×10^{18}	VR5 289 (10-02)	2-D waveguide exp.
3/28/73	13.8	3.0×10^{14}	6×10^{17}	VR5 289 (10-03)	K.W.
4/ 2/73	25	5.4×10^{14}	4×10^{18}	VR5 302 (11-01)	m=0,1 8.75 DB/cm, 9.45
4/ 2/73	25	5.4×10^{14}	4×10^{18}	VR5 302 (11-02)	K.W.
4/ 2/73	13.7	4.6×10^{15}	4×10^{18}	303 (13-01)	erratic coupling
4/ 2/73	18.5	5.8×10^{14}	4×10^{18}	304 (14-01)	Modulation exp.

TABLE VII

GaAs/GaAsP Structures Submitted for Evaluation

Date	Film Thickness μm	Film Carrier Conc. 1cc	Substrate Carrier Conc. 1cc	% ρ	Sample Number	Evaluation Remarks
4/2	<13.7	4.6×10^{15}	1.6×10^{16}	38.6	VR5 303 (12-01)	m=0 3.15 DB/cm
5/4	10.1	9.3×10^{14}	8.1×10^{16}	22.8	VR5 340 (15-01)	m=0,1 1.34 DB/cm, 2.75
5/18	19.5	7.6×10^{14}	8.1×10^{16}	22.8	VR5 347 (16-01)	poor coupling, wafer cracked from excessive bow
5/18	16.6	5.6×10^{15}	1×10^{17}	38.6	VR5 348 (16-02)	m=0,1 1.67 DB/cm, 15.8
5/18	16.6	5.6×10^{15}	1×10^{17}	38.6	VR5 348 (16-03)	not evaluated
5/18	21.2	1.3×10^{15}	5×10^{16}	39.3	VR5 349 (16-04)	not evaluated
5/23	20	6.3×10^{15}	1×10^{17}	38.6	VR5 353 (17-01)	unable to excite a guided wave
5/23	9.8	5.6×10^{15}	8×10^{16}	22.8	VR5 354 (18-01)	m=0, 1 DB/cm
5/23	9.8	5.6×10^{15}	1×10^{17}	38.6	VR5 354 (18-02)	unable to reliably excite guided wave - bowed.
5/24	8.8	3.5×10^{15}	1×10^{14}	38.6	VR5 355 (19-01)	unable to excite guided wave-bowed
5/24	8.8	3.5×10^{15}	8×10^{16}	22.8	VR5 355 (19-02)	poor coupling & erratic results - bowed
5/24	8.8	2.1×10^{15}	8×10^{16}	22.8	VR5 356 (20-01)	m=0 1.8 DB/cm
5/24	8.8	2.1×10^{15}	8.2×10^{16}	34.7	VR5 356 (20-02)	not evaluated
6/8	24.6	2.1×10^{15}	8×10^{16}	22.8	VR5 358 (21-01)	15 DB/cm 0th mode?
6/8	24.6	2.1×10^{15}	8.2×10^{16}	35	VR5 358 (21-02)	not evaluated

E. CONCLUSIONS

1) Relatively high background contamination is due to silicon which is formed principally from reactions of HCl with the quartz reactor.

2) GaAs predeposits act as a getter for the silicon impurities. The background contamination level may be reduced an order of magnitude or more by the predeposition.

3) Ammonia is not an effective agent for reducing the background doping level in GaAs.

4) Modified growth conditions have been developed which produce films with carriers in the mid $10^{14}/cm^3$ range and high mobility.

5) Surface appearance and background contamination are the major problems associated with growing GaAs films on GaAsP substrate.

6) Suitable high resistivity GaAs epitaxial films have not yet been grown reproducibly.

SECTION III

LIQUID PHASE EPITAXY

A. INTRODUCTION

The primary objective of the Liquid Phase Epitaxy (LPE) portion of the program was to grow GaAs/GaAlAs epitaxial layers on GaAs substrates. Since it is easier to grow thin epi-layers with good wurface structure by vapor phase epitaxy, the VPE process will be used to grow the GaAs layer on the GaAlAs LPE layer.

The primary goal of the LPE work is to ascertain whether the GaAlAs system offers a significant improvement in waveguide performance over that obtained with GaAsP or GaAs devices which can be grown using the more highly developed VPE technology.

B. EXPERIMENTAL SYSTEMS

A detailed technical description and performance data of the Radiant Heating Furnace and the large Resistance Diffusion Furnace, controls and gas - handling system were given in the January Semi-Annual Technical Report.

The Radiant Heat Furnace shown in Figure 4 is presently being used to saturate a melt of Ga plus Al with AsH_3 to form GaAlAs. The gas phase saturation usually produces a product with a lower background impurity level than does the addition of undoped GaAs. The gas phase saturation also makes it possible to resaturate a used melt up to the starting growth temperature. The graphite melt saturation boat is shown in Figure 5.

The 12 inch graphite sliding-boat used in the growth of large area GaAlAs epi-layers is shown in Figure 6 and a schematic diagram of the boat is shown in Figure 7. This diagram which was also shown in the January report is repeated here simply to make this report self-contained. Most of the successful growth runs have been made by eliminating the use of source material and growing the epi-layer in the source material slot. The reasons for this change has been the difficulty and expense of obtaining large-area low-impurity GaAs, the occasional slider sticking problems in passing over the source material slot, and the ease of saturating from the vapor phase in the Radiant Heat Furnace system.

Growth runs with the large 12 inch boat were made in a resistance furnace (Lindbergh Hevi-Duty Lancer Diffusion Furnace) with a 20 inch 0.5°C flat temperature zone with programmed cooling as

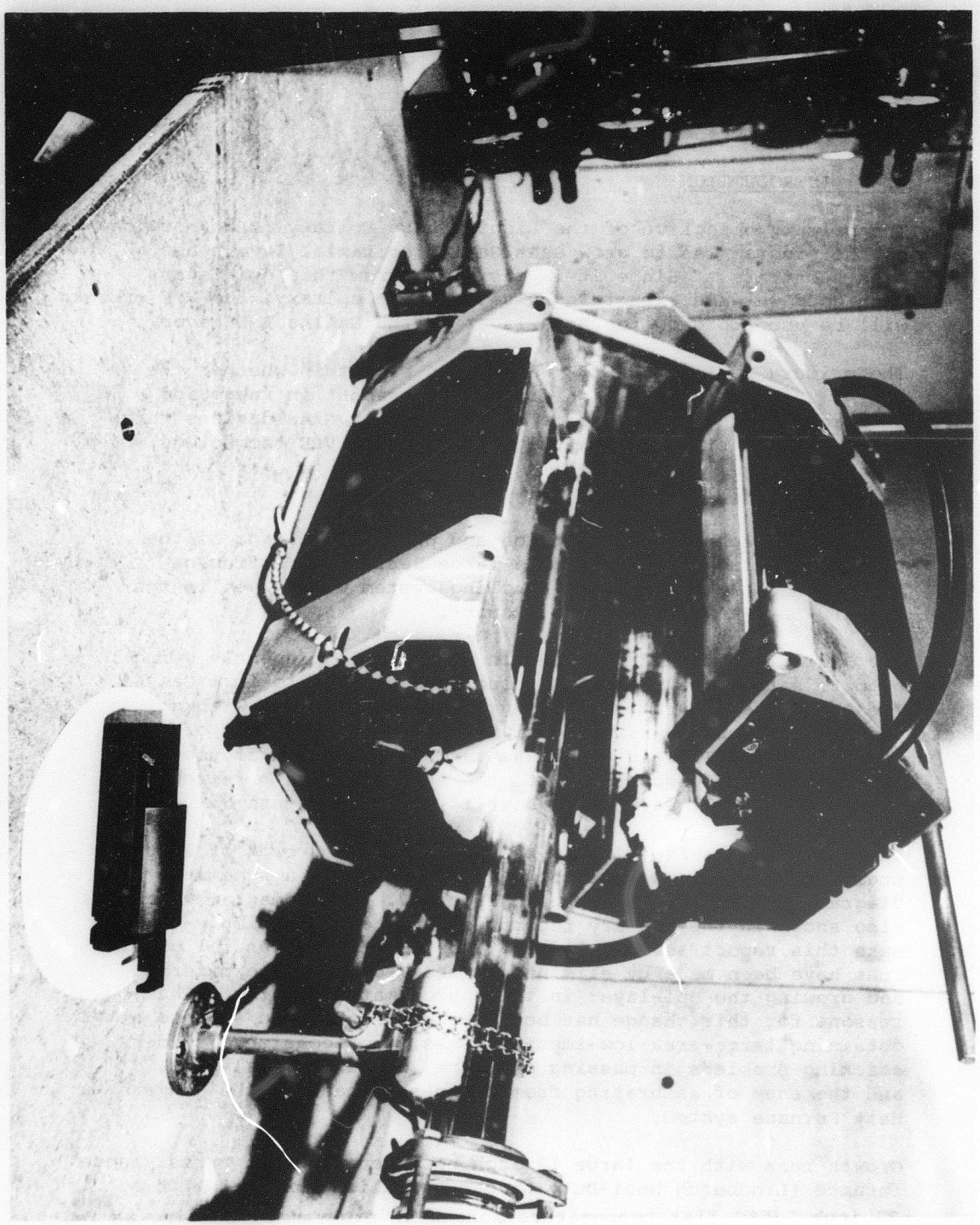

Figure 4 Radiant Heat Furnace and Melt Saturation System

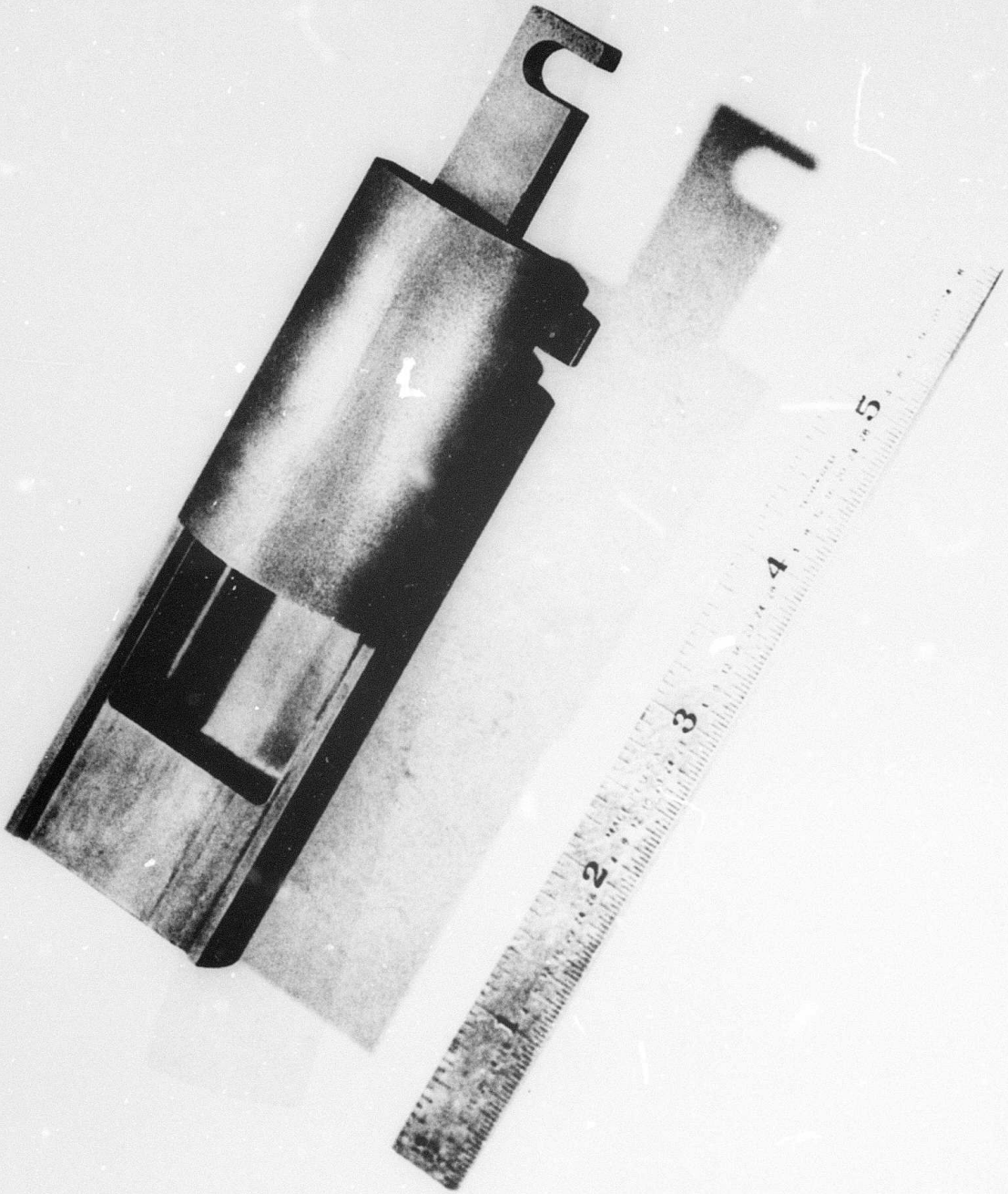

Figure 5 Gas-phase Graphite Melt Saturation Boat

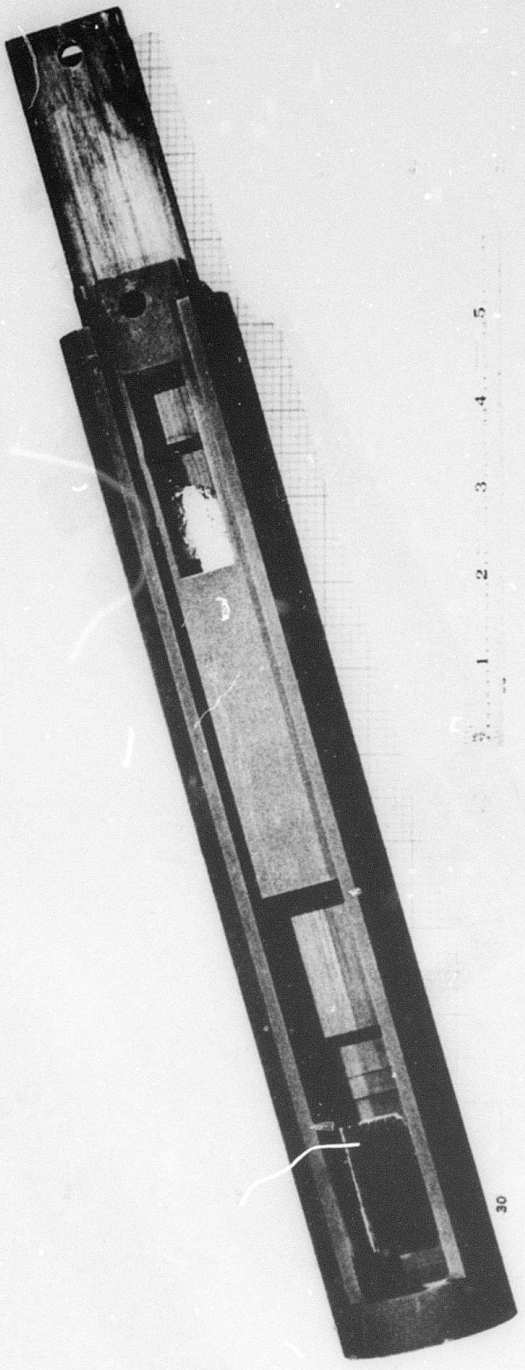

Figure 6 12-inch Graphite Slider Boat for Growth of Larger Area GaAlAs Layers

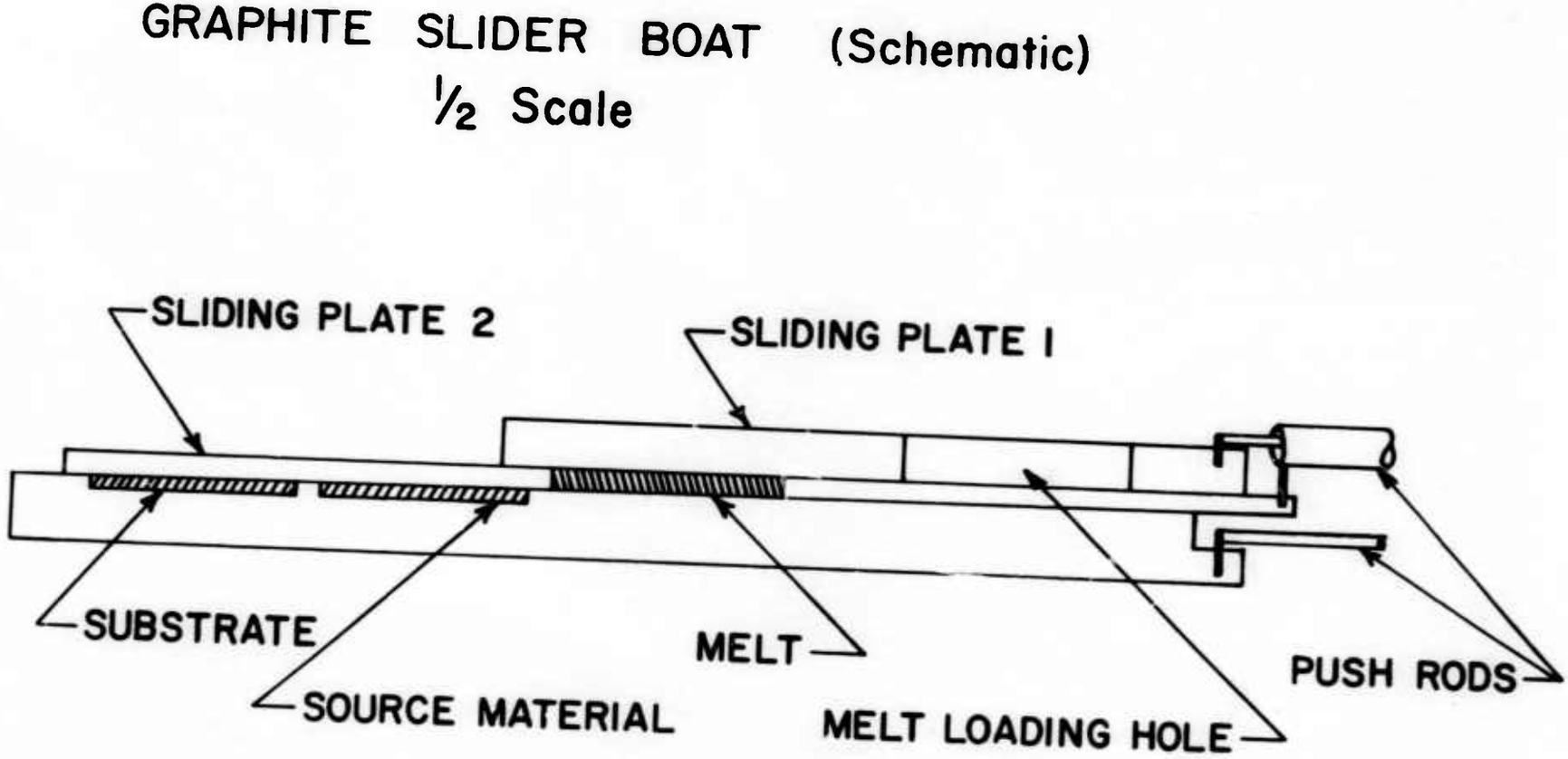

Figure 7 Schematic Diagram of Graphite Sliding-Boat System

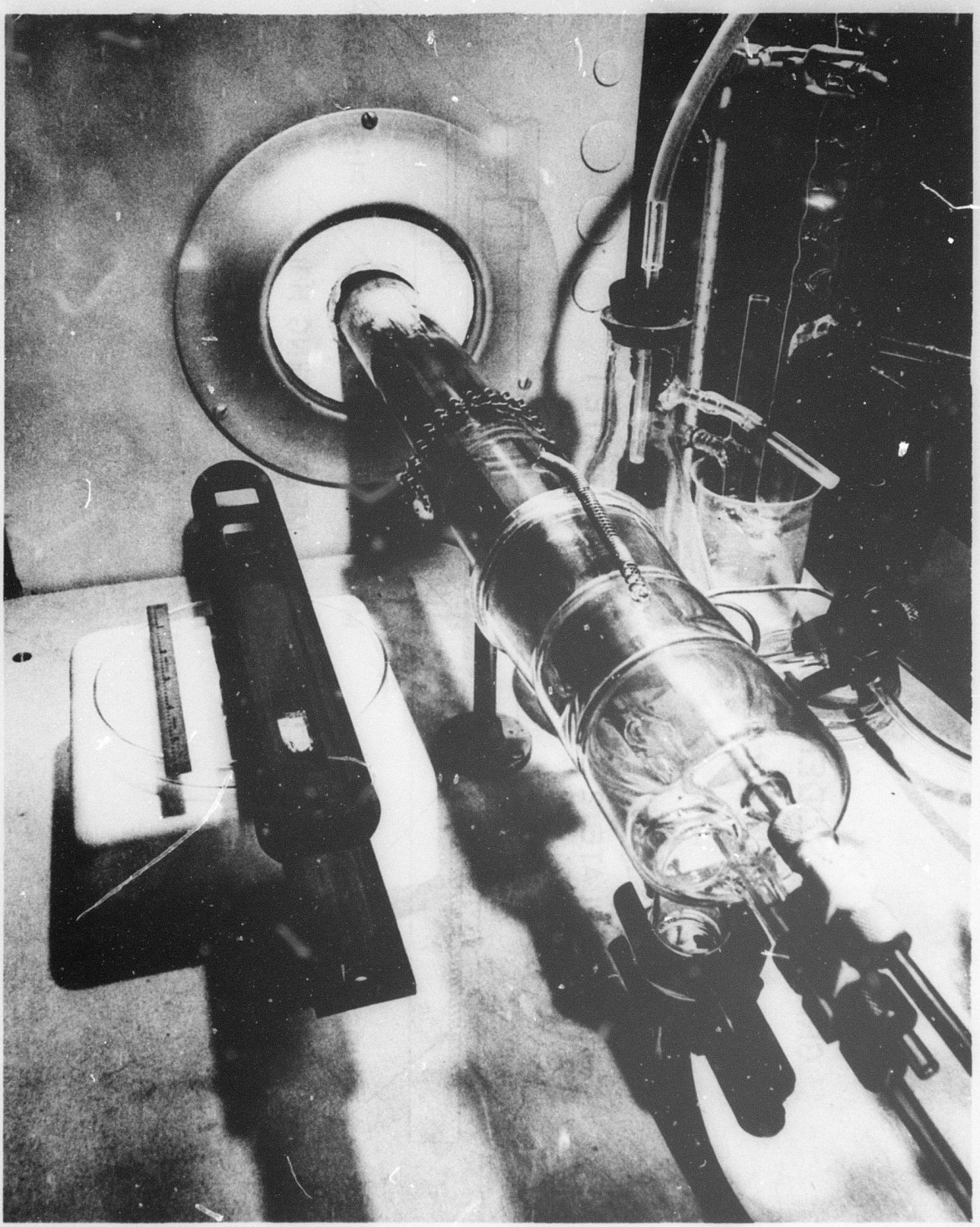

Figure 8 Loading End of LPE Growth Furnace

low as 0.5°C/min. The loading end of the furnace and reactor tube are shown in Figure 8. The control rods provide movement of the boat and sliders while an ambient flow of purified hydrogen is passing through the reactor tube.

C. EXPERIMENTAL RESULTS

Experimental results reported in the January Semi-Annual Technical Report indicated that the relatively small mass of the six inch boat plus the short flat temperature zone of the radiant-heat furnace precludes the growth of large area uniform epi-layers.

A series of runs have now been made in the 12 inch boat using substrates up to 3/4 x 2 inches. In Figure 8, the saturated melt containing the proper amount of Al can be seen in the right cavity and a polished substrate (GaAs) in the depression on the left side of the boat. The bottom slider moves the melt over the substrate for the growth cycle and the top slider covers the melt. After the growth cycle, both sliders are moved to the right to remove the melt from the epi-layer.

The 12 inch boat has produced epi-layers with a greatly improved surface quality and layer uniformity. A schematic drawing of a typical grown layer with a surface composition of 24 mole % AlAs is shown in Figure 9. The measured layer thickness is indicated along a cleavage edge across the wafer. The layer thickness is quite uniform, 24 μm ± 1 μ over most of the wafer with a decreasing layer thickness only at one end where the layer first contacted the melt. The surface quality was reasonably good and, with the addition of a GaAs layer on the surface, would be adequate for preliminary waveguide evaluation.

The successful melt wipe-off action of the slider is critically dependent on the clearance between the slider and the epi-layer surface, therefore the substrate and the layer thickness must be closely controlled. When complete melt wipe-off is obtained, the surface composition is very uniform, as measured by photo-luminescence (PL). When a thin film of melt is left on the surface, a thin layer of alloy low in aluminum is deposited. This layer can be removed by a diamond polish followed by an etch polish. Since the composition gradient in the GaAlAs epi-layer is very steep, a slight nonparallel to the growth surface lapping will result in a small spread in the final surface composition. This deviation has usually been kept at or below ± 1.5 mole % AlAs.

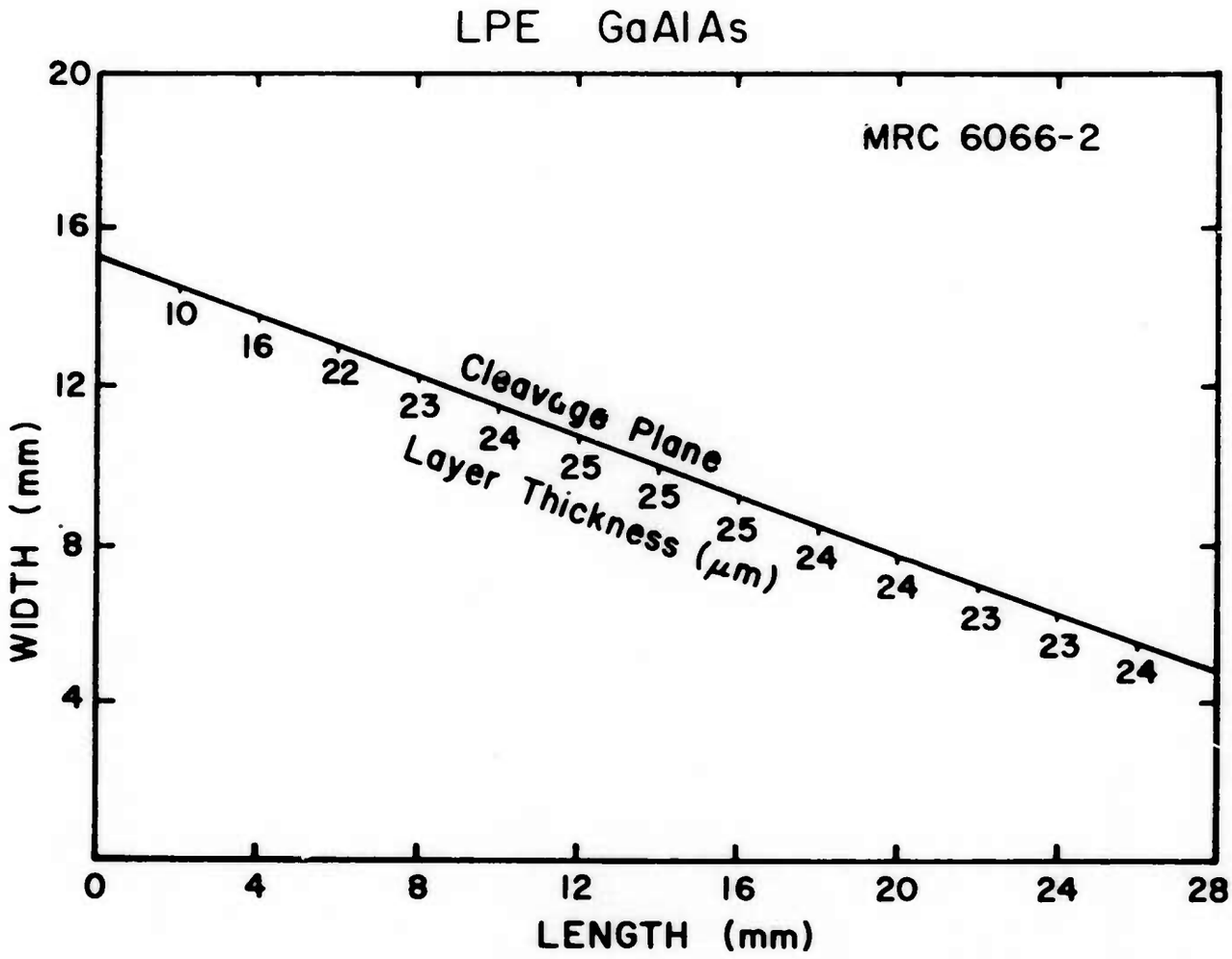

Surface Composition: $GaAl_{.24}As_{.76}$

Epi-layer Carrier Conc: $5.0 \times 10^{16}/cm^3$

Substrate (GaAs) Carrier Conc: $6.8 \times 10^{16}/cm^3$

Figure 9

Typical LPE GaAlAs epi-layer run data obtained from the 12 inch slider boat are given in Table VIII. Large area epi-layers with a surface composition in the range of 20 to 28 mole % AlAs or a $PL_{300°K}$ wavelength of 7450 to 7000Å, respectively, were grown. A saturation or growth starting temperature near 975°C was used. The 30 to 40°C cooling cycle and a cooling rate of 0.5°C/min. resulted in epi-layers with a thickness range of 18 to 27 μm. In most of the runs a small substrate of high resistivity GaAs was included so that a Hall measurement of the epi-layer could be obtained. Most of the layers indicated a carrier concentration in the low 10^{16}a/cc range with a mobility near 1500 cm^2/volt-sec. at room temperature.

Some of the melt charges were reused several times by adding additional aluminum and resaturating with AsH_3. The aluminum addition required was estimated and the saturation temperature was determined by observing the first-crystal formation temperature while the melt was slowly cooled. With some experimental data and a little experience, the surface composition of the epi-layer can be kept near the desired 26 mole % AlAs range.

Most of the GaAlAs layers in Table VIII are ready for the growth of the final GaAs layer by VPE. A series of smaller area GaAlAs epi-layers have also been prepared for the experimental VPE runs required to establish the proper growth conditions for the GaAs layers.

D. CONCLUSIONS

1) GaAlAs epi-layers up to 2 inches in length can be grown in the 12 inch graphite.

2) Several large area GaAlAs epi-layers are ready for the deposition of the final GaAs layer by VPE.

TABLE VIII

TYPICAL LPE GaAlAs GROWTH DATA FROM THE LARGE-AREA SLIDER BOAT SYSTEM

Run No. MRC-	Al added (g)	Saturation Temp. (°C)	Cooling Rate (°C/min)	Growth Range (°C)	Epitaxial Layer Thickness (μm)	Epitaxial Layer Carrier Conc. (a/cc)	Epitaxial Layer Mobility $\left(\frac{cm^2}{V.sec.}\right)$	Epitaxial Layer PL* Wavelength (Å)	Remarks
6065	50	975	0.5	30	27	9.4×10^{16}	1580	7450	New 25g Ga charge
6066	28	970	0.5	35	24	5.0×10^{16}	1640	7215	Resaturated melt from above
6067	50	977	0.5	35	~35	----	----	----	New 25g Ga charge, melt did not wipe clean, PL after etch polish=7100 to 7300Å
6068	60	973	0.8	40	~28	2.2×10^{16}	1473	----	New 25g Ga charge, melt did not wipe clean, PL after etch polish-6800 to 7100Å
6069	50	978	0.5	30	~34	5.8×10^{16}	1505	----	New 25g Ga charge, Melt did not wipe clean, PL after etch polish=6900 to 7100Å
6070	30	973	0.5	30	20	------	----	7330	Resaturated melt from above

Continued

TABLE VIII CONTINUED

Run No. MRC-	Al added (g)	Saturation Temp. (°C)	Cooling Rate (°C/min)	Growth Range (°C)	Epitaxial Layer Thickness (μm)	Epitaxial Layer Carrier Conc. (a/cc)	Epitaxial Layer Mobility $\left(\frac{cm^2}{V.sec.}\right)$	Epitaxial Layer PL* Wavelength (Å)	Remarks
6071	34	970	0.5	30	20	----	----	7040	Resaturated melt from above, p/n junction 5μ from interface
6072	30	960	0.5	30	18	1.3×10^{16}	----	7140	Resaturated melt from above
6073	54	980	0.5	30	33	5.2×10^{15}	1671	7200	New 25g Ga charge
6074	30	970	0.5	35	21	1.5×10^{16}	1547	7100	Resaturated melt from above
6075	30	960	0.5	35	18	1.6×10^{16}	1074	7000	Resaturated melt from above

*(PL) = Photoluminescence at surface of epi-layer (300°K).

SECTION IV

WAVEGUIDE EVALUATION

A. MEASURED AND CALCULATED WAVEGUIDE ATTENUATION

More attenuation rate measurements were made on different waveguides.

The data of several GaAs/n^+GaAs waveguides, for different TE modes, are shown by the points marked by their mode order in Figure 10. The solid curves in Figure 10 represent the theoretically calculated attenuation rates for the various TE modes in GaAs/n^+GaAs waveguides as a function of thickness. In this calculation the film is considered to be intrinsic and the substrate carrier concentration is 4×10^{18} carrier/c.c. In Figure 11 the attenuation data of the TE_0 mode is replotted. This figure gives a general assessment of the effect on attenuation rate caused by the change in thickness without regard to the free carrier concentrations in the different substrates ($8 \times 10^{17} < N_s < 4 \times 10^{18}$). The solid curve in Figure 11 represents the averaged characteristics of the experimental data. The two triangular points are experimental data for the GaAs/$GaAs_{1-x}P_x$ waveguides do not exhibit this sharp increase in attenuation at small film thicknesses. Figure 12 is a comparison of the experimental data (the crosses) on two GaAs/GaAsP waveguides with the theoretically calculated attenuation rate (the solid curves). Here the free carrier concentration in $GaAs_{1-x}P_x$ is 8×10^{16} and the x is 0.228, corresponding to a $\Delta n \cong 0.09$. The agreement between experimental and theoretical results are good for the m = 0 mode and not so good for the m = 1 mode. There are only two propagation TE modes in these waveguides.

The data then qualitatively demonstrates the advantage of alloy structures for GaAs waveguide. More data on GaAs/GaAsP waveguides, as well as new data on GaAs/GaAlAs data, will be collected so that a full comparison of the three structures can be made in December, 1973.

A paper was presented at the 1973 CLEA conference on the comparison of GaAs/GaAsP and GaAs/n^+GaAs waveguides. A written paper will be prepared during the next period when a more complete set of data on GaAs/GaAsP waveguides are collected. The problem of how to reduce the residual waveguide attenuation to less than 1 db/cm still exists. The experimental evaluation of this problem will be delayed until better surface quality films with low carrier concentrations can be obtained reproducibly from the material growth program.

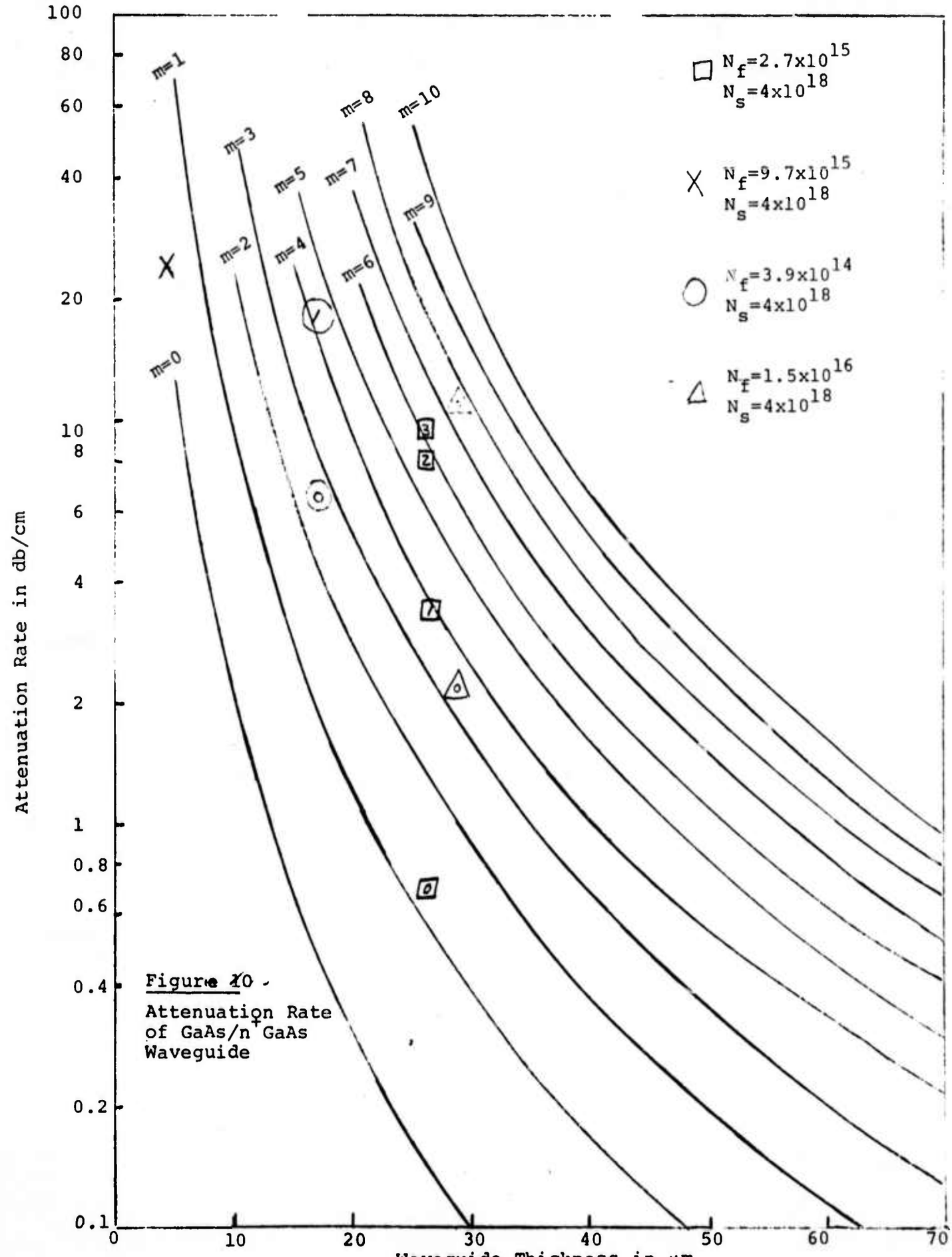

Figure 10 -
Attenuation Rate of GaAs/n$^+$GaAs Waveguide

Figure 11 Attenuation Rate of TE_o Mode in GaAs/n^+GaAs Waveguides

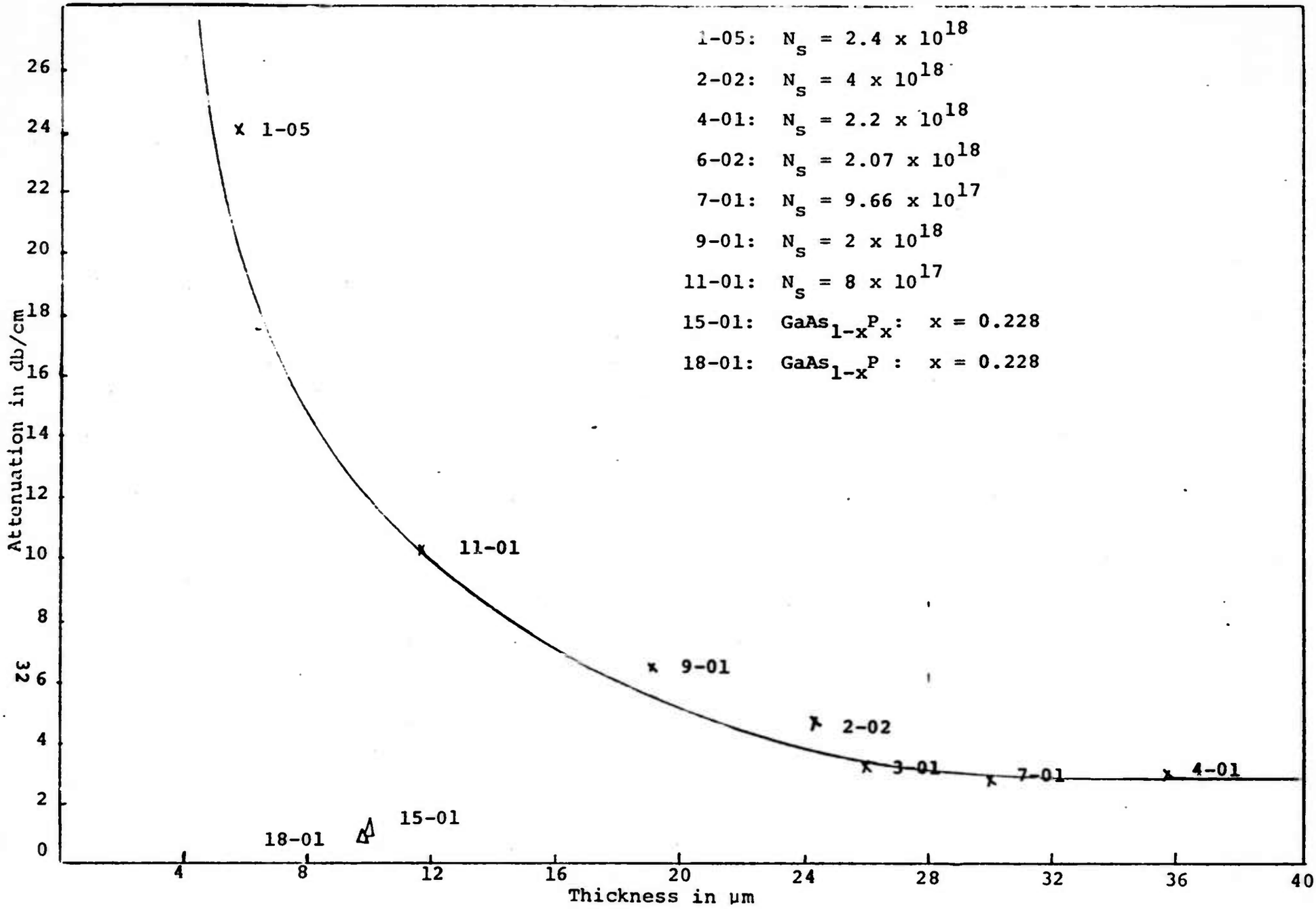

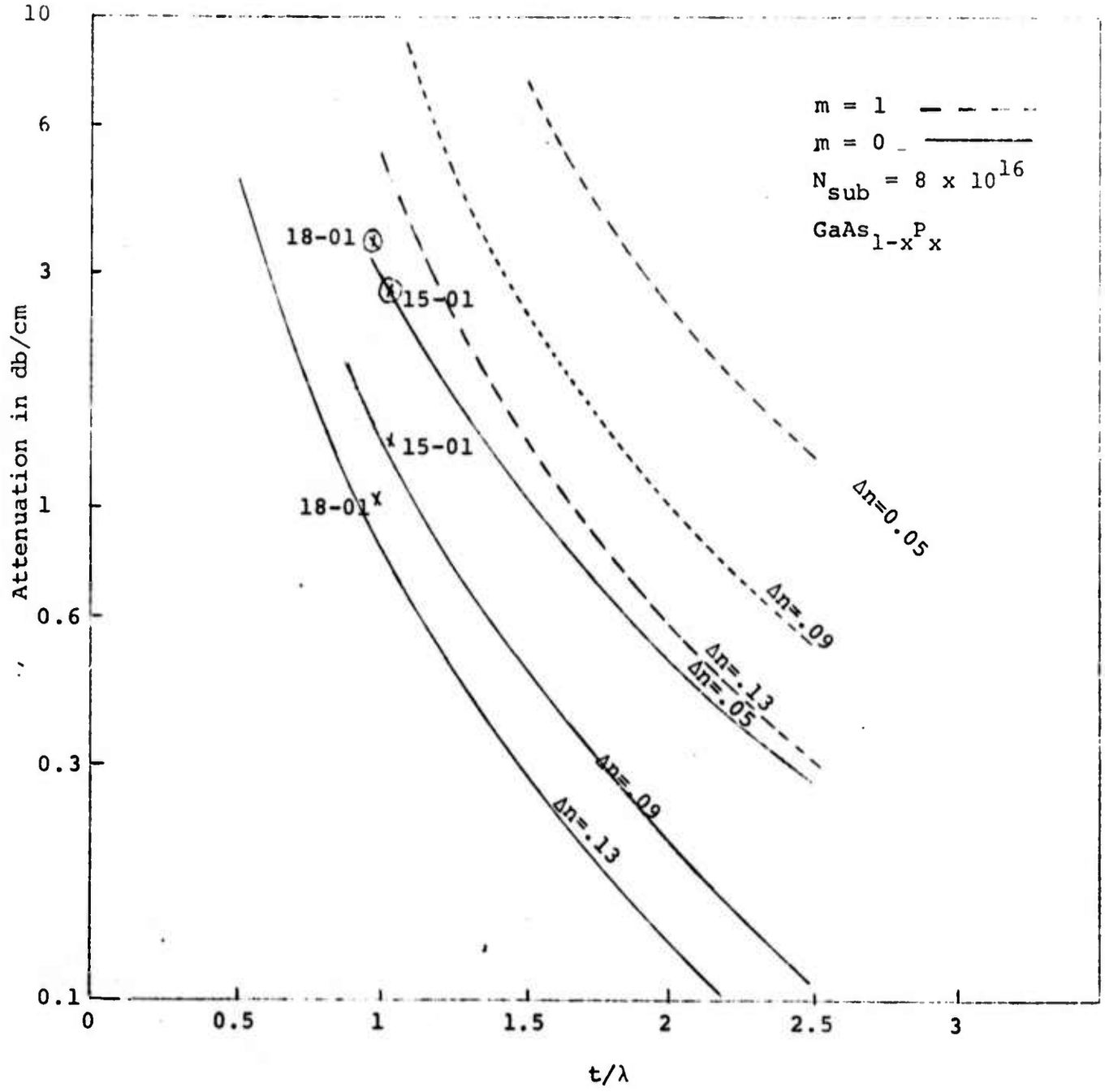

Figure 12 Attenuation Rate of GaAs/GaAsP Waveguides

B. ANALYSIS OF WAVEGUIDES WITH GRADED INDICES OF REFRACTION

The analysis of the propagation wave number β for each mode with uniform refractive index in the film and linear variation of the refractive index in a given transition region has been completed. Numerical results have been obtained which indicate that as far as the calculation of β is concerned the waveguide with a graded index of refraction can be represented by an equivalent uniform film waveguide having an effective thickness w_0. Figure 13 shows an example of the calculated results. In this figure, a contour map of the ratio of β of the TE_0 mode to the free space propagation wave number, k, is presented as a function of the film thickness w and transition region thickness d at 10.6 μm wavelength. These are GaAs/n^+GaAs waveguides with $N_s = 10^8$ carrier/c.c. substrate carrier concentrations. An extension of the analysis has also been made to calculate the field configuration for the mode. From the field calculation, the attenuation rate of the waveguide was calculated and presented in Figure 14. Figure 14 shows the attenuation rate curves for the TE_0 mode for the waveguides that have the w and the d values corresponding to the specific β/k values shown in Figure 13.

The calculation demonstrated that with the transition region measured to be less that 1μ thick for most of the GaAs abrupt layer waveguides, the effect of the transition region on β and on attenuation rate can be neglected. The calculated results will be used as a guide for the fabrication and evaluation of graded index guides later in the contract.

C. DEVICE EVALUATION

A theoretical comparison of the effectiveness of the various electro-optical modulation schemes in GaAs epitaxial waveguides has been made in the NSF grant. The results were reported in the Berkeley NSF Grantees' Conference on Optical Communication in 1973 and are attached here as Appendix I to the semiannual report. There are several implications on the GaAs epitaxial waveguide that can be drawn from the appendix.

1) In order to reduce both the voltage and the modulation power per unit bandwidth requirements for electro-optical modulation, small film thickness waveguides must be employed. Since the GaAs/n^+GaAs waveguides have excessive attenuation for waveguides less than 10 μm thick, only GaAs/GaAsP or GaAs/GaAlAs waveguides are suitable for this kind of application.

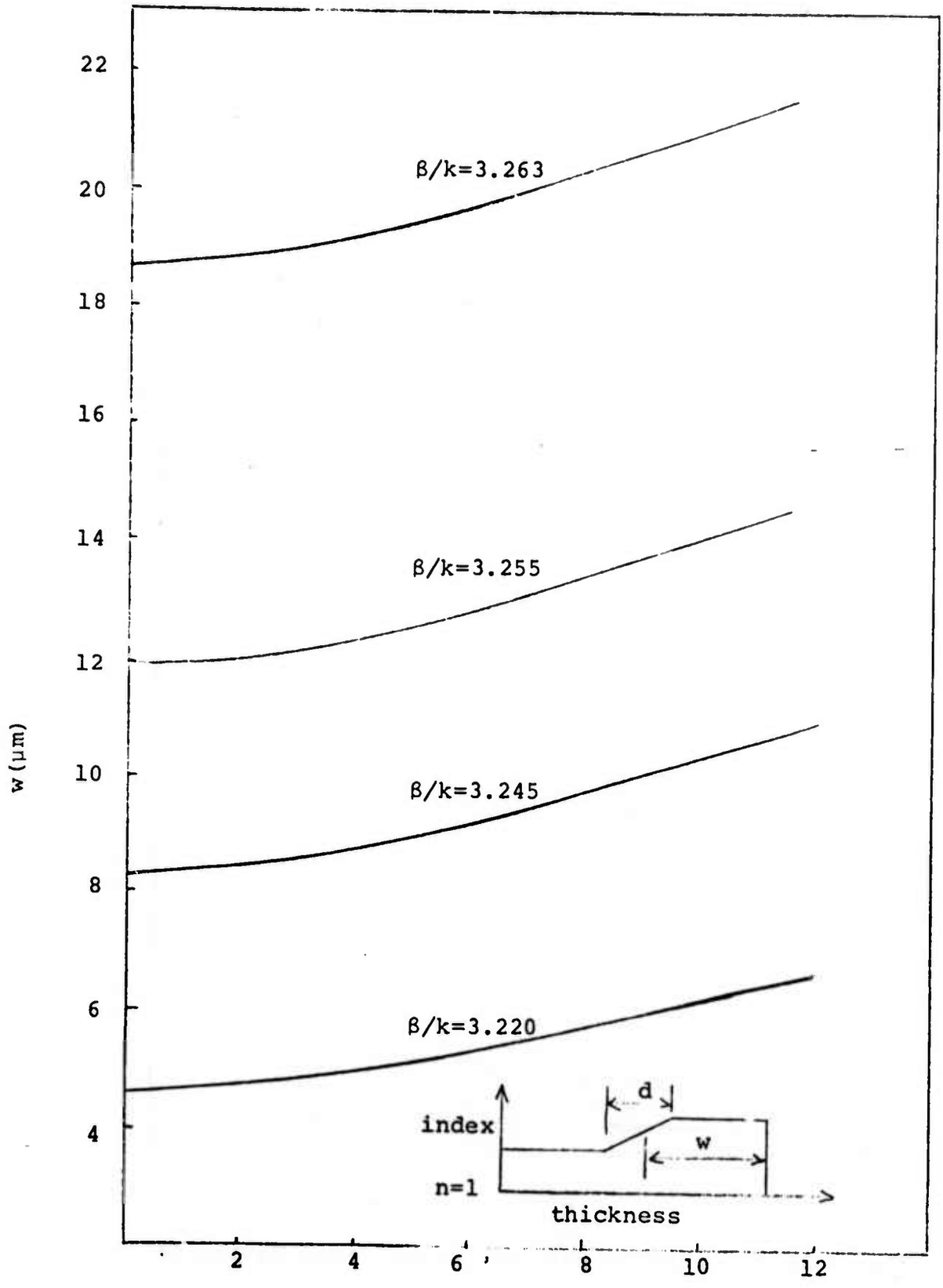

Figure 13 Contour Map of β for Graded Refractive Index Waveguide

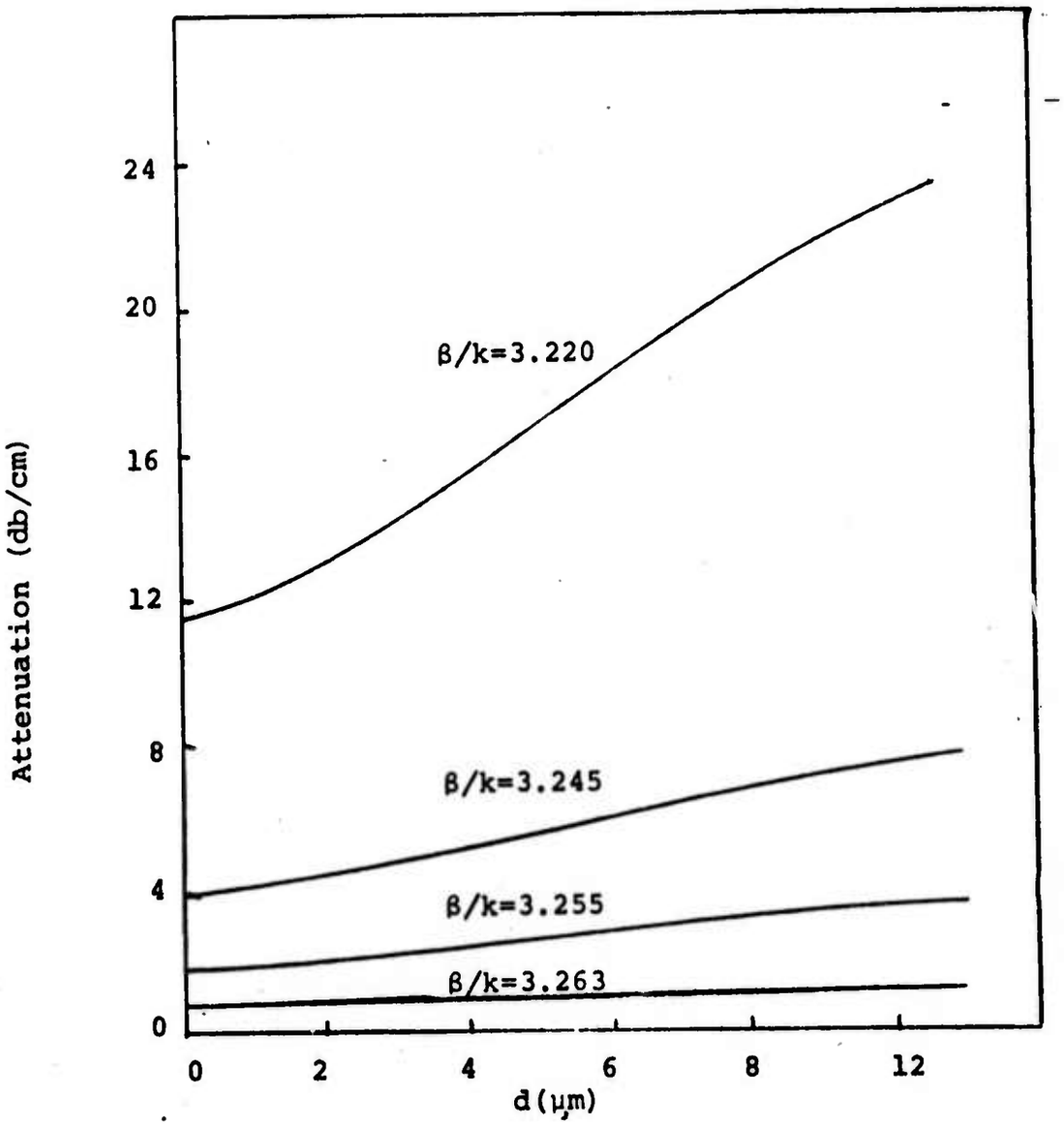

Figure 14 Attenuation Rate of Graded Index Waveguide

2) There is an optimum film thickness that will allow us to modulate with the lowest voltage r.f. power. Hence, control of film thickness in the growth process of the epitaxial film will be important.

3) Due to avalanche breakdown, there is an upper limit on the r.f. voltage that can be applied to the modulator. Assuming that both the maximum allowed voltage and the optimum waveguide thickness are used, we still need several centimeters of interaction length in the waveguide for either π-phase or 100% amplitude modulation. Therefore, the material growth program should strive for large sample size (5 cm or longer).

4) The efficiencies of the phase modulation, Bragg's modulation, and backward wave modulation schemes are comparable to each other. But the efficiency of the forward mode conversion scheme is lower than these other schemes due to the small value of its overlap integral.

5) The large r.f. capacitance of the one-dimension uniform thin film waveguides is the major reason for the substantial power per unit bandwidth required in one dimensional guided wave modulators. Although its required r.f. power is already substantially lower than that of the corresponding bulk modulator, this r.f. power can be reduced further if the capacitance can be reduced by using a two dimensional waveguide with narrow guide width. More recent calculation performed in the NSF grant indicate theoretically that a reduction of power by a factor of 40 is realizable in two dimensional waveguides.

These considerations led us to launch two experimental programs in this contract. One program is to demonstrate and to evaluate electro-optical modulation experimentally. The second program is to evaluate the attenuation rate of two dimensional waveguides.

D. EXPERIMENTAL DEMONSTRATION OF ELECTRO-OPTICAL MODULATION

Experimentally, based upon the calculated results shown in the appendix and based upon an available waveguide already fabricated, we have designed a Bragg's modulator.

Initially, a mask consisting of grating fingers, 1 cm long, 31.8 μm in periodicity, and 10.2 μm wide was fabricated by usual photolithography technique. This mask was used to fabricate an aluminum electrode pattern on a GaAs epitaxial waveguide by the

photo-lift-off method[3]. Due to the lack of high enough resistivity epitaxial film at the present time, it was decided that the best technique to obtain electro-optical deflection is to make the grating electrode into a Schottky barrier. If a d.c. reverse biased voltage is applied to the electrode, it whould allow us to create the electro-optical effect without excessive modulation power dissipation in the waveguide. Unfortunately, the total needed area of the Schottky barrier electrode is approximately 1/3 cm^2. With such a large area there is a high probability that some defects in the film or in the fabrication process will create localized high electric field regions. Because of these defects we were only able to get a reverse bias breakdown voltage of less than 15V in the first modulator fabricated, while small test Schottky barriers made on the same film showed a reverse bias breakdown voltage larger than 100V. With only 10V applied to the electrode, no modulation effects were observed in the first modulator.

To eliminate the difficulty caused by defects under a large Schottky barrier electrode, we redesigned the mask into groups of three individual grating fingers as shown in Figure 15a.

An SiO_2 layer was first deposited on a new piece of waveguide (13.7 μm thick GaAs on n^+GaAs substrate). A set of aluminum grating electrodes shown in Figure 15b was then made on top of the SiO_2 pattern and the GaAs by the lift-off method using the mask shown in Figure 15a. Each group of grating finger is then tested electrically for its reverse breakdown individually. Less than 10% of the grating finger groups were found to have a low reverse breakdown voltage. These bad grating finger groups were marked, and an interconnecting mask as shown in Figure 15c was made, designed specially to connect only the good grating finger groups together to the applied modulation voltage. This mask was then used to fabricate an interconnecting electrode to connect just the good grating fingers. In this manner we avoided the defects that caused the low reverse breakdown voltage. The grating periodicity and the phase matching conditions will not be affected seriously by the omission of the bad grating fingers as long as the percentage of bad ones is small. The SiO_2 layer insures us that no defect under the connecting electrode will cause a low reverse breakdown voltage. Figure 16 illustrates the completed electro-optical modulator. Figure 17 shows the microscopic photograph of the grating pattern, the SiO_2 pattern, and the interconnection electrode. A reverse bias voltage of over 70 volts was obtained in this modulator.

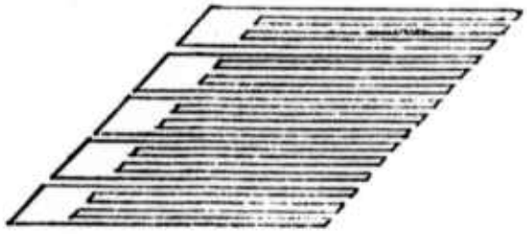

(a) The Electrode Mask

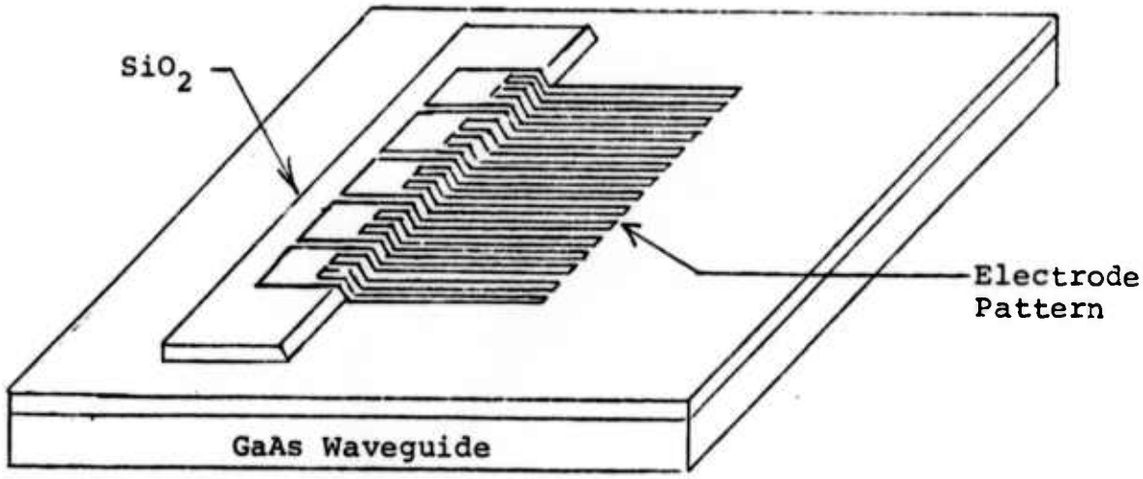

(b) The Electrode with SiO_2 Insulation

(c) The Interconnecting Electrode Mask

Figure 15 Illustration of the Fabrication Processes for Bragg's Modulation Electrode

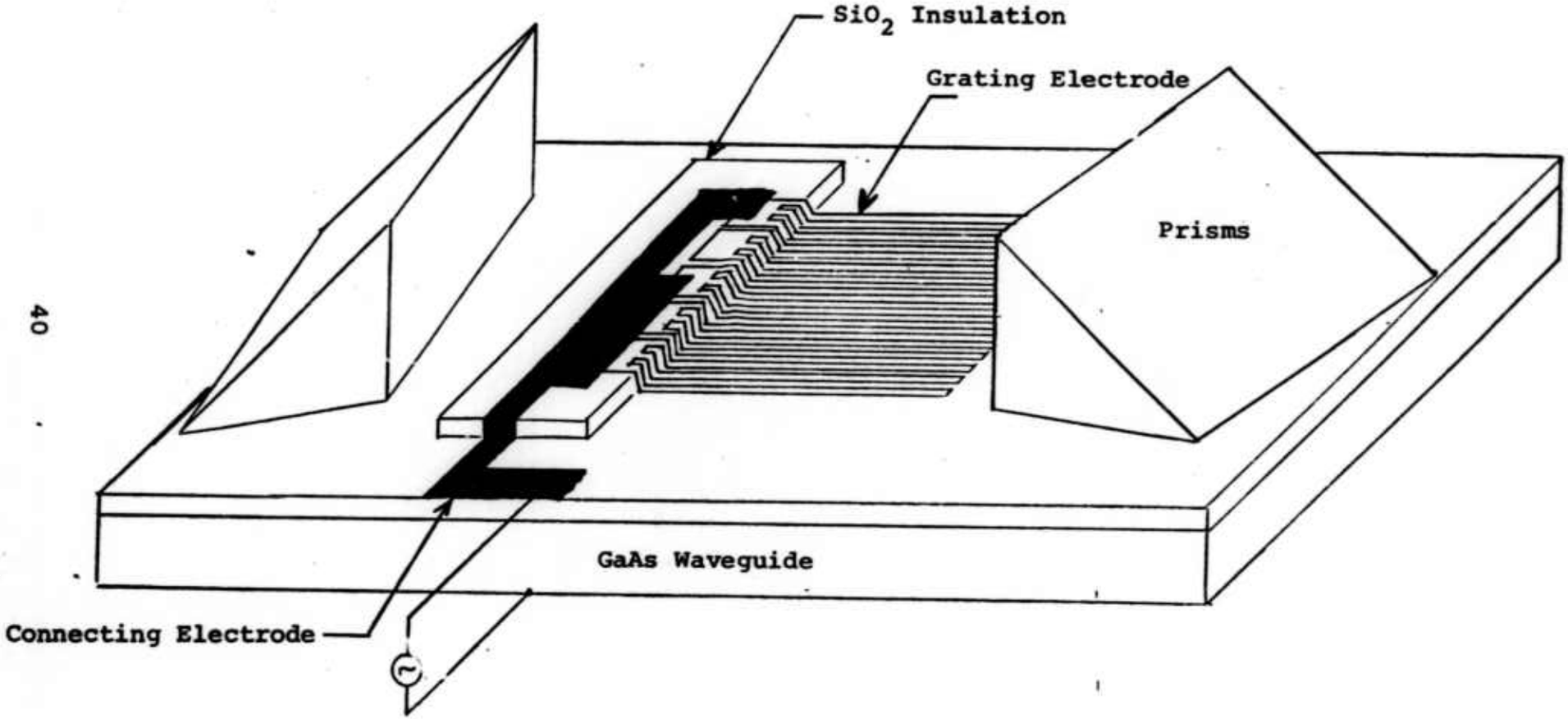

Figure 16 Illustration of Bragg's E-0 Modulator

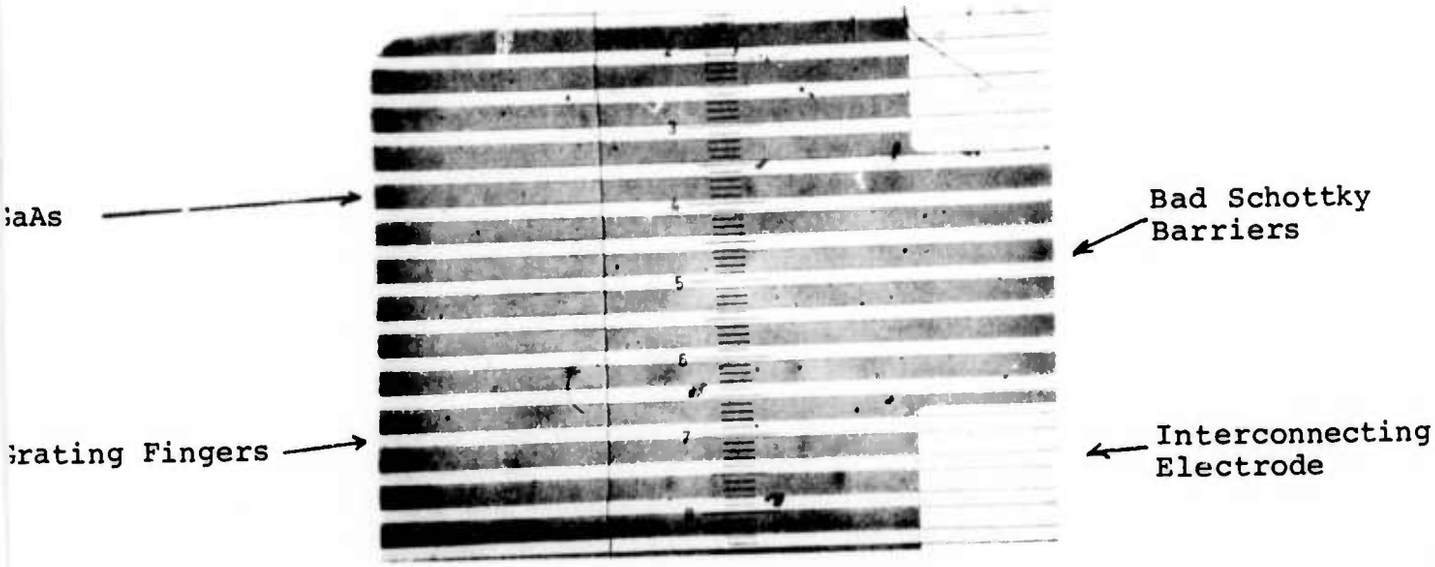

Figure 17 Microscope Picture of the Grating Electrodes

Subsequently, a guided wave was excited and detected by the prism input and output coupler. When the input prism is oriented in the direction that will launch an incident guided wave satisfying the Bragg's condition with the known periodicity and grating orientation of the electrode and when a reverse bias voltage is applied to the grating electrode, both a change in the propagation of the incident guided wave and a deflected guided wave along the expected Bragg's direction of deflection was observed. In order to increase the sensitivity of the detection scheme, the reverse bias voltage was chopped in synchronism with a reference voltage; phase sensitive detection was employed so that even a small change in incident power or a small deflected power could be measured. According to the results given in the appendix, we should have less than 1% efficiency in deflection for 60V of applied voltage and 1 cm of interaction length for the waveguide employed (13.7 μm film in an n^+GaAs substrate). Experimentally we measured the deflection efficiency to be somewhere between 0.1% and 1%. Theoretically a thin waveguide (say 5 μm thick) together with grating fingers of 5 cm long should yield a deflection efficiency of more than 50% at 60V of applied modulation voltage

In short, we have successfully demonstrated the Bragg's electro-optical modulation. The efficiency is low because we used an existing structure that is not optimized for this application. In the next period, a special GaAs/n^+GaAs structure will be grown and tested with a 2 cm long grating pattern to obtain more efficient modulation and to check our theoretical results.*

E. EXPERIMENTAL FABRICATION OF TWO DIMENSIONAL WAVEGUIDES

The results given in the appendix and the more recent theoretical results indicate that for low laser power communication applications, a large reduction in r.f. power may be obtained by using two dimensional waveguides to reduce the capacitance and the required r.f. power of the modulator. However, it is well known that the attenuation rate of the etched two dimensional waveguide in the visible light is very high due to the scattering loss from the rough side wall. Yet, the scattering loss due to rough side walls

* The SiO_2 layer will cause additional attenuation of the waveguide at 10.6 μm wavelength. The SiO_2 insulation pattern is used temporarily to demonstrate the modulation effect. In the actual design of a practical modulator, the SiO_2 pattern will be eliminated and the metallic grating electrode will be separated from the guiding film by a buffer GaAsP or GaAlAs film.

should decrease dramatically for the longer 10.6 μm wavelength. Therefore, the usefulness of two dimensional waveguides can only be established after careful experimental investigations.

A two dimensional waveguide was fabricated experimentally with an epitaxial film of 13.8 μm thick on an n^+GaAs substrate having carrier concentrations of 10^{18} carrier per c.c. The width of the waveguide is 35 μm wide. The fabrication was done by means of chemical etching using the usual photolithography technique and a chromium mask, without making any special effort to get high resolution in the chromium mask pattern or in the etching process. The measured attenuation rate was a pleasant surprise of 13 db/cm.

We are greatly encouraged by this result. A program has been launched to experiment with different metal films for high resolution mask and to try different etching methods including both chemical and sputtering processes. This effort will be reported during the next period.

F. CONCLUSIONS

1) More attenuation rate data were collected for the GaAs/n^+GaAs and the GaAs/GaAsP waveguides. These data demonstrated the advantages of the alloy structures for GaAs waveguides at 10.6 μm wavelength.

2) Analysis of Waveguides with Graded Indices of Refraction has been completed.

3) The theoretical comparison of the various electro-optical modulation schemes in GaAs epitaxial waveguides has assisted us to direct the material growth program to strive for the following goals:

   a) Thin alloy waveguides
   b) Large sample sized (5 cm or longer)
   c) High resistivity films
   d) Controlled waveguide thickness
   e) Low loss two dimensional waveguides

4) Preliminary demonstration of Bragg's diffraction electro-optical modulation in GaAs waveguides has been obtained.

5) Work in two dimensional waveguide has been initiated.

SECTION V

WORK FOR NEXT PERIOD

During the next six months of the project the following tasks will be undertaken:

A. VAPOR PHASE EPITAXY

1) Improve surface quality of GaAs n/n+ and GaAs/GaAsP samples.

2) Reduce carrier concentration in the GaAs layer of the GaAs/GaAsP samples.

3) Grow preliminary GaAsP/GaAs/GaAsP samples for evaluation.

4) Grow VPE GaAs layers on LPE GaAlAs substrates for a preliminary comparison of GaAs/GaAsP and GaAs/GaAlAs material systems.

5) Continue efforts to grow compensated high resistivity GaAs.

B. LIQUID PHASE EPITAXY

1) Continue work to improve surface quality of grown epitaxial layers.

2) Attempt to reduce carrier concentration of GaAlAs epitaxial layer.

C. WAVEGUIDE EVALUATION

1) Continue evaluation of GaAs/GaAsP and GaAs/GaAlAs structures, as they become available, and make preliminary comparison of GaAs/GaAsP, GaAs/GaAlAs, and GaAs n/n+ systems.

2) An experimental demonstration of the electro-optical amplitude modulation via Bragg's diffraction scheme designed to have an improved modulation efficiency (10% to 30% range) will be carried out, utilizing a specially designed wave guide structure. The data from this experiment will be used to check the theoretical analysis completed in the NSF grant for electro-optical modulation in GaAs epitaxial waveguides.

3) A few two-dimensional waveguides will have been prepared using chemical and sputter etching. Preliminary results will be obtained.

4) A technical report on the results of the theoretical calculation of attenuation rates for both the abrupt and the graded refractive index waveguides will be prepared for GaAs/n^+GaAs, GaAs/GaAsP, and GaAs/GaAlAs waveguides.

REFERENCES

1. K. L. Lawley, et al., "Manufacturing Methods for GaAs", Final Technical Report #AFML-TR-71-55, March, 1971.

2. P. L. Hoyt and R. W. Haisty, "The Preparation of Epitaxial Semi-Insulating Gallium Arsenide by Iron Doping", J. Electrochem. Soc. 113, 296-297, (1966).

3. H. I. Smith, F. J. Bachner, and N. Efremow, "A High-Yield Photolithographic Technique for Surface Wave Devices", Journal of the Electrochemical Society 118, 821, (1971).

APPENDIX I

A COMPARISON OF ELECTRO-OPTICAL MODULATION METHODS IN GaAs EPITAXIAL THIN WAVEGUIDES AT 10.6μm WAVELENGTH

by

Ton Ko and W. S. C. Chang

Department of Electrical Engineering

and

Laboratory for Applied Electronic Sciences

Washington University

St. Louis, Missouri 63130

(NSF Grant GK 31854)

Technical Report - 73-6

I. Introduction

For linear electro-optic effects the change in refractive index along the direction of the transverse electric field, to a good approximation, can be written as[1]

$$\Delta n = -\frac{1}{2} n^3 r E \tag{1}$$

where r is the electro-optical coefficient, E is the amplitude of the applied electric field for modulation, and n is the refractive index.

Consider now a waveguide consisting of an epitaxially grown layer of intrinsic GaAs on top of an n^+GaAs substrate having a carrier concentration from 10^{16} per c.c. to 10^{18} per c.c. (or $GaAs_{1-x}P_x$ or $GaAl_yAs_{1-y}$). The mth TE guided wave mode propagating in the z direction is described by

$$E_y = E_m(x) e^{-j\beta_m z} e^{j\omega t} \tag{2}$$

A similar equation can be written for E_x of the TM modes.

If a pair of electrodes is fabricated on the top of the film and on the bottom of the substrate as shown in Figure 1, a Δn will be created whenever a voltage is applied to the electrodes. Since the substrate has much lower resistivity than the film, very little voltage drop will appear across the substrate. Thus,

$$\Delta n_2 \cong 0 \tag{3a}$$

$$\Delta n_1 \cong -\frac{1}{2} n_1^3 r \, (V/d) \tag{3b}$$

where d is the thickness of the epitaxial film.* When the refractive index of the film is changed from n_1 to $n_1 + \Delta n_1$, a new propagation wave number β_m' is obtained, $\beta_m' = \beta_m + \Delta\beta_m$. Thus a net phase shift of ϕ_m is obtained in a modulator of length ℓ, where [2],[3]

$$\Delta\phi_m = \Delta\beta_m \ell \tag{4}$$

For the GaAs waveguides, we calculated analytically the $\Delta\beta_m$ and obtained

$$\phi_m = C_m \ell V \tag{5a}$$

$$C_m = \frac{k^2 n^4 r}{2\beta_m d}\left[\frac{\beta_m}{2\omega\mu}\int_0^d E_m E_m dx\right] \tag{5b}$$

where $k = 2\pi/\lambda$ and the quantity in the bracket representing the fractional power of the mth mode contained in the film, n_1 is the normalized overlap integral for the electro-optical interaction.

Phase modulation is the simplest method for electro-optical modulation. However, it is only useful in a homodyne (hetrodyne) communication system. In order to obtain amplitude modulation, one could

---

*If the attenuation of metallic electrode on top of the epitaxial film is excessive, a lower resistivity buffer layer of epitaxial GaAs (or $GaAs_{1-x}P$ or $Ga_{1-y}Al_yAs$) 2 or 3 μm thick can be added to the waveguide before the deposition of the electrode. This will not affect our calculated results of Δn_1 significantly.

either interfere the phase modulated beam by another reference beam or obtain the amplitude modulation directly from Bragg's diffraction or mode conversion methods.[4] It would be important to compare the performance of phase modulation with these two methods quantitatively.

Figure 2 shows an electro-optical Bragg's diffraction modulator.[5],[6] It is similar to the phase modulator, except now the top electrode has the grating pattern. When a voltage is applied across the grating-like electrodes, there will be a periodic variation of the refractive index, Δn_1 (i.e. we will have a Bragg's phase grating). It is well known that a Bragg's phase grating will diffract the energy in the incident mth TE mode to the nth TE mode in a new direction of propagation whenever

$$\underline{\beta}_m - \underline{\beta}_n = \pm \underline{K} \tag{6}$$

where $K = \frac{2\pi}{L}$; $\underline{K}$ is directed perpendicular to the grating grooves; $\underline{\beta}_m$ and $\underline{\beta}_n$ are directed in the direction of propagation of the mth and the nth modes. When both the incident and the diffracted waves are TE_m modes, $\underline{K}$ is approximately perpendicular to $\underline{\beta}_m$ and $\underline{\beta}_n$ with

$$K = 2\beta_m \sin \psi \tag{7}$$

Here ψ is the angle of diffraction.

Figure 3 shows the grating electrode pattern of a mode conversion modulator where $\underline{K}$ is approximately parallel to $\underline{\beta}_m$. Here, similar to Bragg's diffraction, the mth and nth mode will be coupled if

$$\underline{\beta}_m - \underline{\beta}_n = \pm K \tag{8}$$

In this case $\underline{\beta}_m$ can be approximately parallel to $\underline{\beta}_n$ (called forward mode conversion) or antiparallel to $\underline{\beta}_n$ (called backward mode conversion) depending upon the magnitude of K.

II. Modulation Efficiency

A perturbation analysis has been carried out using Maxwell's equations concerning the Bragg's diffraction and mode conversion methods.[7] The results of this analysis can be summarized as follows:

(a) Because Δn_1 is very small, there will be very little radiation loss caused by the grating.

(b) Let R be the amplitude of the TE_m mode incident on the grating modulator and S be the amplitude of the diffracted mode caused by the grating. Let the width of the metallic finger of the grating electrode be $\frac{1}{2}$ of the grating periodicity L and ℓ be the length of of the grating modulator. Let R be one at z = 0 and S be zero at z = 0 for Bragg's diffraction and forward mode conversion (S = 0 at z = ℓ for backward mode conversion). Then for Bragg's diffraction

$$R = \cos\left[\frac{1}{\pi}(\cos\psi)C_m \ell |V(t)|\right] \tag{9a}$$

$$S = j\sin\left[\frac{1}{\pi}(\cos\psi)C_m \ell |V(t)|\right] \tag{9b}$$

For backward mode conversion,

$$R = \operatorname{sech}\left[\frac{1}{\pi}(\cos\psi)C_m \ell |V(t)|\right] \tag{10a}$$

$$S = j\tanh\left[\frac{1}{\pi}(\cos\psi)C_m \ell |V(t)|\right] \tag{10b}$$

For forward mode conversion,

$$R = \cos\left[\frac{1}{\pi}(\cos\psi)\ell |C_{mn}V(t)|\right] \tag{11a}$$

$$S = j\sin\left[\frac{1}{\pi}(\cos\psi)\ell |C_{mn}V(t)|\right] \tag{11b}$$

$$C_{mn} = \frac{k^2 n^4 r}{2\beta_m d}\left[\frac{\beta_m}{2\omega\mu}\int_0^d E_m E_n dx\right] \tag{11c}$$

Here we have assumed that in the case of Bragg's diffraction and backward mode conversion, the diffracted mode is still the TE_m mode, while the diffracted mode in the forward mode conversion case is a TE_n mode. Figures 4 and 5 show a plot of the $\frac{1}{2\pi} C_o V\ell$ and $\frac{1}{2\pi} C_{o1} V\ell$ as a function of waveguide thickness for $n_{film} = 3.27$, $n_{substrate} = 3.127$, and for $n_f = 3.27$, $n_{substrate} = 2.14$.

From Equations (5), (9), (10), and (11), it is clear that modulation and diffraction efficiency of the different schemes are simply different functions of the variable $C_o V\ell$ or $C_{o1} V\ell$; hence, we can plot the efficiency for different schemes of electro-optical modulation on the right side of Figures 4 and 5, adjusting the scale to fit the different functions. The dashed curve represents the limitation on the applied r.f. voltage due to avalanche breakdown for ℓ = 1 cm.

Three important conclusions can be drawn from Figures 4 and 5. They confirmed quantitatively our earlier qualitative expectation that in order to have efficient electro-optical modulation at reasonable voltages, one needs to have long modulators (4 or 5 cm long) and thin epitaxial waveguides. In terms of the GaAs waveguides, this means that GaAs/n^+GaAs waveguide will not be suitable because of its large attenuation due to free carrier absorption in the substrate. The GaAs/$GaAs_{1-x}P_x$ or GaAs/$Ga_{1-y}Al_yAs$ will be of prime importance. Secondly, they showed that forward mode conversion will be the least efficient of all the schemes for lumped element electro-optical modulation (an extension to traveling wave modulation will be discussed in Section IV. This is caused primarily by the small value for the overlap integral. Thirdly, they showed that, due to the increase of evanescent tail in the substrate region, when the waveguide thickness is decreased, there is a maximum efficiency for a given V and ℓ at an optimum waveguide thickness. Hence, control of film thickness

as well as fabrication of long waveguide structures and low attenuation rates are important.

III. Driver Consideration in Electro-Optical Modulation

In all of the modulators just described it is necessary to apply a time varying electric field to the electrodes in order to achieve r.f. modulation. We must estimate the amount of r.f. power needed to drive such a modulator

For V volts applied across a GaAs waveguide modulator, the voltage drop appears mostly across the high resistivity epitaxial layer. Hence the electric field in the film is

$$E = V/d \tag{12}$$

the resistive component of the current density is

$$J = E/\rho \tag{13}$$

The equivalent circuit of the modulator at the radio or microwave frequency is, effectively, the parallel combination of the capacitance of the dielectric filled electrode structure and its resistance. For

$$V = V_o \sin \omega_m t \tag{14}$$

we obtain

$$P_d = \frac{V_o^2 A}{2\rho d} = \text{r.f. power dissipated in the modulator} \tag{15}$$

A is the cross sectional area of the electrode.

Let there be a r.f. source having source resistance R_s.

This source is coupled to the modulator in parallel with a load resistor R_L through an ideal transformer as shown in Figure 6. The voltage across the modulator will drop to $\frac{1}{\sqrt{2}}$ of its low frequency value at the frequency

$$\Delta\omega = \frac{2}{CR} = 2\pi\Delta f \tag{16}$$

where R is the parallel combination of the modulator and the load resistance. $\Delta\omega$ is customarily interpreted as the bandwidth of the modulator. Usually, one minimizes the power dissipated in the modulator by using large values of ρ and obtains the necessary bandwidth $\Delta\omega$ by adjusting R_L. The power delivered to the modulator and the load resistor is a maximum when $R_s = R$. In that case

$$P = \frac{V_o^2}{2R} = \frac{V_o^2}{4} C\Delta\omega \tag{17}$$

Thus, the power required to drive the modulator per unit bandwidth is [8]

$$\frac{P}{\Delta f} = \pi C V_o^2/2 \quad \text{(Watts/Hz)} \tag{18}$$

For a phase modulator with electrons of area $A = w\ell$, epitaxial layer thickness d, and π phase shift, this becomes

$$\frac{P}{\Delta f} = \frac{1}{72}\,\varepsilon_r\,\left(\frac{w}{\ell}\right)\left(\frac{\lambda}{n^3 r}\right)^2\left(\frac{\beta_m}{nk}\right)^2 \frac{d}{\left[\frac{\beta_m}{2\omega\mu}\int_0^d E_m E_m dx\right]^2} \qquad (19)$$

(m watts/MHz)

For a Bragg's diffraction and mode conversion, modulators of area $A = \frac{1}{2}\,w\ell$, epitaxial layer thickness d, and $\frac{1}{\pi}\,(\mathrm{Cos}\psi)\,C_m \ell V_o = \pi$

$$\frac{P}{\Delta f} = \frac{(\pi^2/8)}{72\,\mathrm{Cos}^2\psi}\,\varepsilon_r\,\left(\frac{w}{\ell}\right)\left(\frac{\lambda}{n^3 r}\right)^2\left(\frac{\beta_m}{nk}\right)^2 \frac{d}{\left[\frac{\beta_m}{2\omega\mu}\int_0^d E_m E_n dx\right]^2} \qquad (20)$$

for forward mode conversion

$$\frac{P}{\Delta f} = \frac{(\pi^2/8)}{72\,\mathrm{Cos}^2\psi}\,\varepsilon_r\,\left(\frac{w}{\ell}\right)\left(\frac{\lambda}{n^3 r}\right)^2\left(\frac{\beta_m}{nk}\right)^2 \frac{d}{\left[\frac{\beta_m}{2\omega\mu}\int_0^d E_m E_m dx\right]^2} \qquad (21)$$

for Bragg's and backward mode conversion

These results are plotted in Figure 7. Comparing these P/Δf requirements with the P/Δf of the bulk modulators, we see that there is a large reduction in r.f. power for guided wave modulators. We could now obtain 100 MHz bandwidth modulation

with only 200 to 300 watts of r.f. drive power. However, this power requirement is still very large; it is cumbersome to use hundreds of watts of power to drive the modulator in the 100 MH_z range. If we can reduce the width, w, of the electrode, an order of magnitude or more, we could then obtain GHz of bandwidth with reasonable r.f. drive power.

Another source of difficulty in driving thin film waveguide modulators relates to their impedance and the power disspation in the modulator. Let a typical electrode pattern have d = 10μm, electrode area, $A_o = 10^{-4}m^2$; Equation (15) predicts that for V_o = 50 volts, the r.f. power disspated in the modulator will only be less than 12.5 watts if ρ is larger than 10^5 ohm-cm.

For a modulator to operate with bandwidth Δω, we need the total resistance consisting of the modulator in parallel with load resistor to be

$$R = \frac{\Delta\omega}{2} C = \frac{\Delta\omega}{2} (\varepsilon_o \varepsilon_r \frac{A}{d})$$

For $A = 10^{-4}m^2$, d = 10μm, ε_r = 13, $\Delta f = 10^9$, R is 3.6 ohms. But the impedance of the modulator and the load resistor, seen by the r.f. generator, is*

$$Z = \frac{R}{1 + j2\omega/\Delta\omega}$$

---

*We have assumed here that ρ is high enough; $\frac{d}{A} > R$.

Therefore, the r.f. impedance will be very low (much lower than 50 ohms unless C can be reduced). From Equations (9), (10), and (11) it is clear that d and ℓ will be dictated by the optical modulation efficiency. We must again reduce w in order to have a reasonably large Z for a given desired bandwidth $\Delta\omega$.

In short, from both the impedance and the $P/\Delta f$ points of view, we need to reduce w in order to improve the performance of the electro-optical modulators. This could be achieved by means of two-dimensional waveguides as sketched in Figure 8. For example, a reduction of w from 2×10^{-3}m to 20×10^{-6}m will reduce the capacitance 100 times. With a reduction of C by 100 times we could then extend the modulator to lower GHz of modulation frequency.

Two-dimensional waveguides may have higher attenuation rates than the one-dimensional waveguides. It may also require larger modulation voltage due to a further decrease in the value of the overlap integral. These are the topics under investigation by this grant and by the ARPA contract. We have already etched a two-dimensional waveguide and obtained an experimental attenuation rate of 13 db/cm in the first trial. Further theoretical investigation of different modulation schemes in two-dimensional waveguides will be performed in the next NSF grant period.

IV. Traveling Wave Electro-Optical Modulation

The bandwidth of the lumped modulator discussed in Sections II and III will be limited further by transit time of the optical wave and the wavelength of the modulation r.f. field. Let the modulator have length ℓ, then it is well known that due to the transit time its bandwidth Δf must be smaller than $\frac{2.82}{\ell}\left(\frac{c}{\beta_m k}\right) \cong \frac{2.82}{n_1 \ell}$. Hence, $\Delta f < 2.5 \times 10^9$ Hz for $\ell = 10$ cm and $\Delta f < 5 \times 10^9$ Hz for $\ell = 5$ cm. The modulator must also be much shorter than $\frac{1}{4}$ of microwave wavelength in order to view it as a lumped electrical element. For GaAs, this means $\Delta f << .226 \times 10^8/\ell$. When $\ell = 10$ cm, $\Delta f << \ell \times 10^9$ Hz; and when $\ell = 5$ cm, $\Delta f << 4.5 \times 10^9$ Hz. In short, the lumped modulator is only applicable up to one GHz or less of modulation frequency. We have done a preliminary analysis in this grant to extend the bandwidth to higher GHz range via traveling wave interactions. The results of this analysis can be presented as follows:

Let β_o and ω_o be the propagation wave number and frequency of the nth TE mode. β_{mod} and ω_m are the propagation wave number and frequency of the modulation field propagating parallel to the mth mode. If the waveguide structure can support another TE_ℓ mode that has a propagation wave number at ω_s, that can be propagated parallel to the mth mode and that satisfies the phase matching condition

$$\omega_m = \omega_o - \omega_s$$

$$\beta_{mod}\ (\omega_m) = \beta_n\ (\omega_o) - \beta_\ell\ (\omega_s)$$

Then synchronous interaction between the mth and the ℓth mode will occur.

The effect of the traveling modulation wave is to produce a traveling change of the permittivity of the waveguiding layer according to

$$\Delta n_1 = -\frac{1}{2} n^3 r \, E \, \text{Cos} \, (\omega_m t - \beta_{mod} z)$$

Where E is the peak modulating field. This perturbation leads to a set of coupled differential equations relating the amplitudes of the nth and the mth guided modes. The solution to these equations is again

$$R = \text{Cos} \, [C_{n\ell} \, \ell V] \, \text{Cos} \, (\omega_o t - \beta_n z)$$

$$S = \sin \, [C_{n\ell} \, \ell V] \, \text{Cos} \, (\omega_s t - \beta_\ell z)$$

Where $C_{n\ell}$ is given in Equation (11c), V is the voltage of the modulation subcarrier. For a c.ω. subcarrier modulation field, only a constant amount of energy is converted from the nth mode to the ℓth mode. But when the subcarrier is modulated, V is a function of time and amplitude modulation of R is obtained. Modulated subcarrier is equivalent to the summation of its Fourier components. Hence, in order for the modulation to have wide bandwidth, the phase matching condition must be

satisfied by all the Fourier components. The condition for such a wide band phase matching was found to be

$$\frac{\partial \beta_{\ell}}{\partial \omega_s} = \frac{\partial \beta_{mod}}{\partial \omega_m}$$

In other words, the group velocities of the guided optical structure and the modulating structure must also be matched.

Since the modulating subcarrier is propagating along the same waveguide as the optical guide waves, the power needed to obtain 100% modulation is for the power transmitted through the waveguide to have a voltage V_o that will make $C_{mn} \ell V_o = \frac{\pi}{2}$. Thus

$$P = \frac{V_o^2}{2Z_o}$$

where Z_o is the characteristic impedance of the traveling wave structure at the modulation frequency. For a TEM modulation mode, and for high ρ values, the Z_o can be taken as

$$Z_o = \frac{120\pi}{\sqrt{\epsilon_r}} \left(\frac{d}{w}\right)$$

For example, when $d = 10\mu m$, $w = 2mm$, $Z_o = 0.5$ ohms. Hence, power needed to obtain 100% modulation is

$$\rho = \frac{\sqrt{\epsilon_r}}{960\pi} \left(\frac{wd}{\ell^2}\right)\left(\frac{\lambda}{n^3 r}\right)^2 \left(\frac{\beta_m}{kn_1}\right)^2 \frac{1}{\left[\frac{\beta_m}{2\omega\mu} \int_o^d \epsilon_n \epsilon_{\ell} \, dx\right]^2}$$

Comparing this result with the P/Δf of the lumped modulator, we see that much more modulation power is needed for traveling wave modulator. Once more, a large reduction of modulation power would be required if w can be decreased by using a two-dimensional waveguide. One could get much more reasonable impedance value if w is decreased. Moreover, one could also get an interaction length much longer than 5 cm, if one uses a zig-zag path for the two-dimensional waveguide.

IV. Experiments on Electro-Optical Modulation

Experimentally, the evaluation of electro-optical modulation must depend upon the availability of high resistivity epitaxial films. An alternative way to obtain the high resistivity is to make the metal electrode into a reverse biased Schottky barrier, so that the depletion layer coincides with the waveguide. However, in this second case, some random defects will likely occur under a large Schottky barrier area ($\sim\frac{1}{2}$ cm^2); they will severely limit the voltage that can be applied to the electrode. Much of these difficulties is associated with the material problem of the GaAs waveguides. Therefore, most of the initial experimental investigation of electro-optical modulation is being carried out in the AFCRL/ ARPA contract.

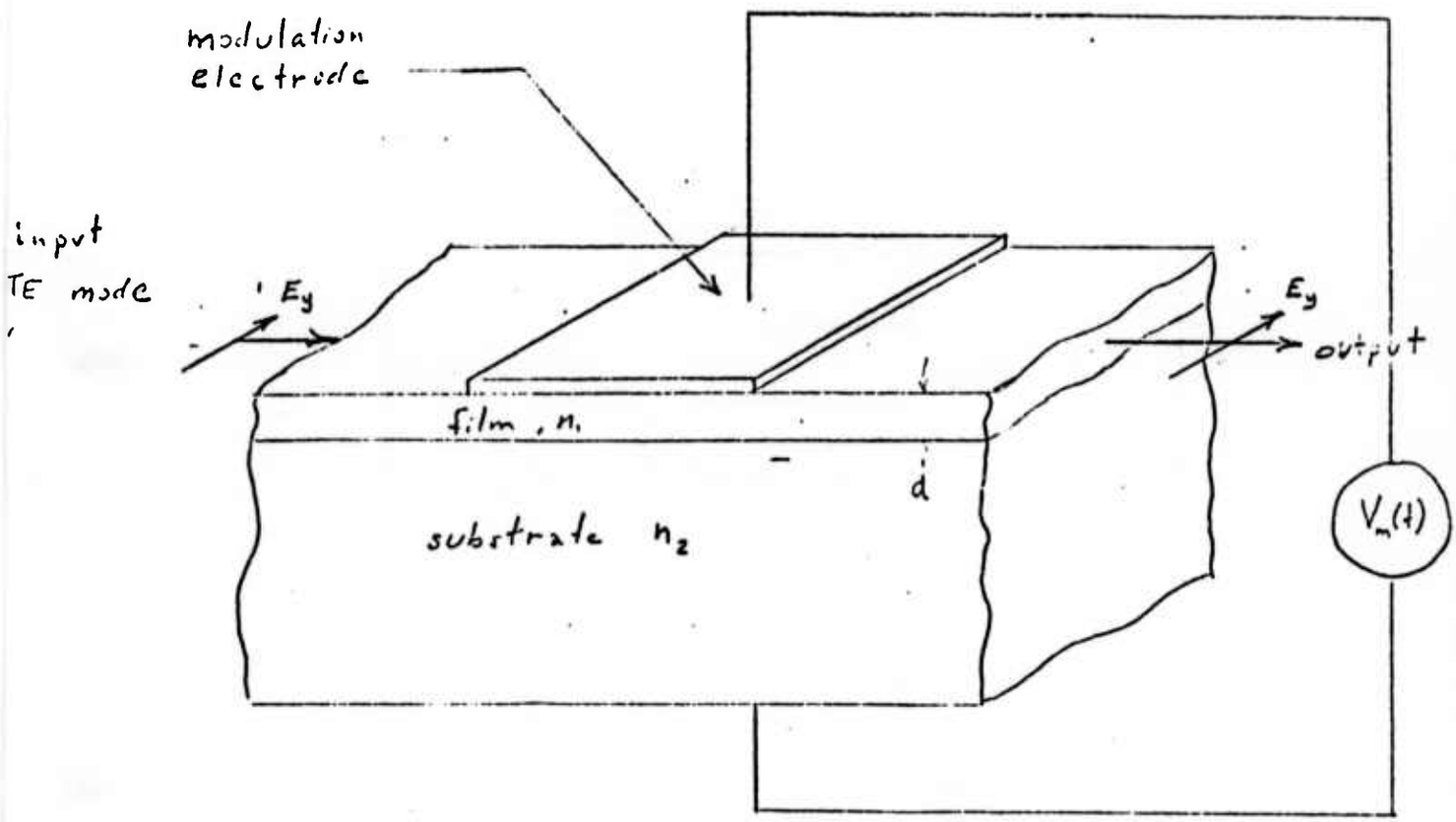

Fig. 1 ε - 0 Phase Modulator

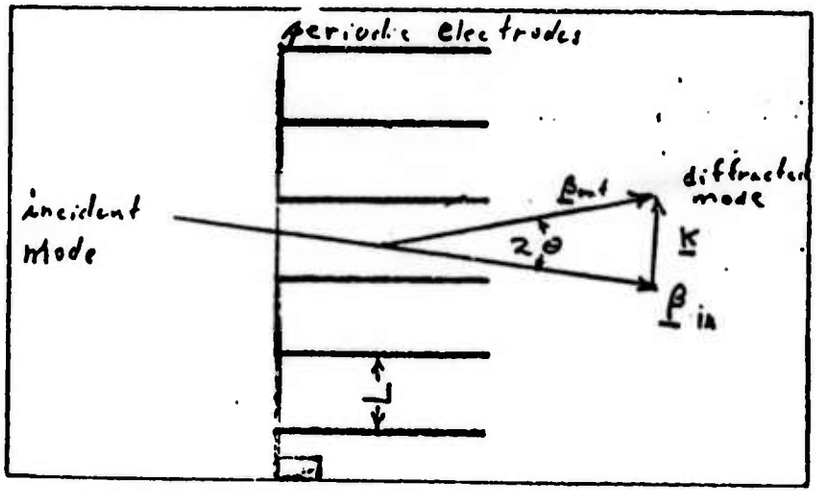

Fig. 2 Top View of Electro-optical Bragg's Diffraction Modulator

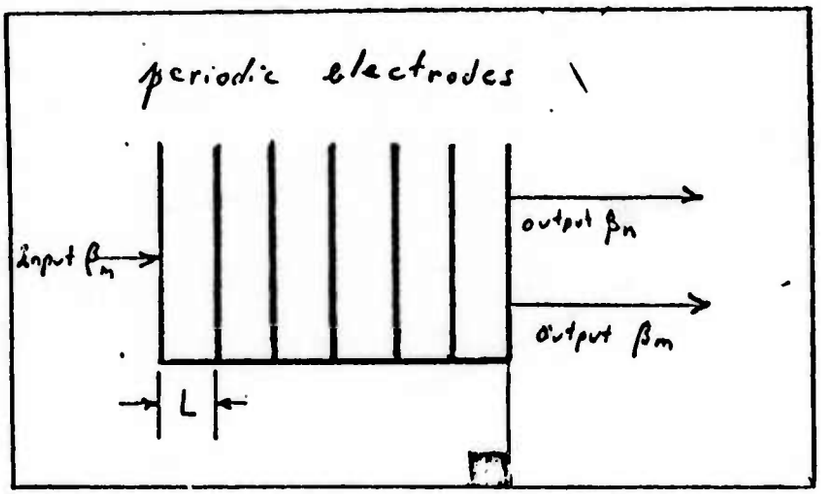

Fig. 3 Top View of Collinear Electro-optical Mode Conversion Modulator

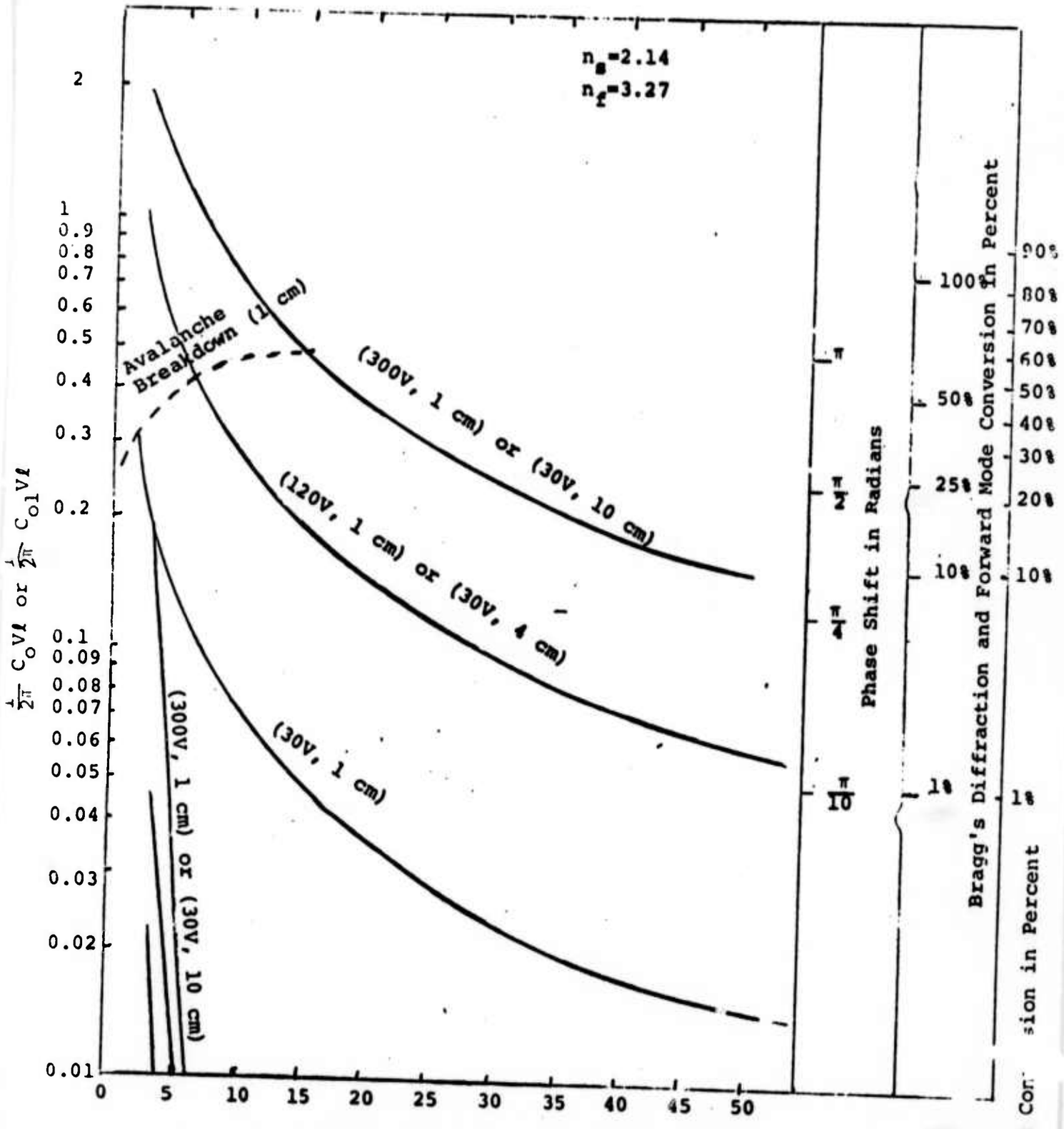

Fig. 4 Modulation Efficiency of Various Modulation Schemes
(n_f = 3.27 n_s = 2.14)

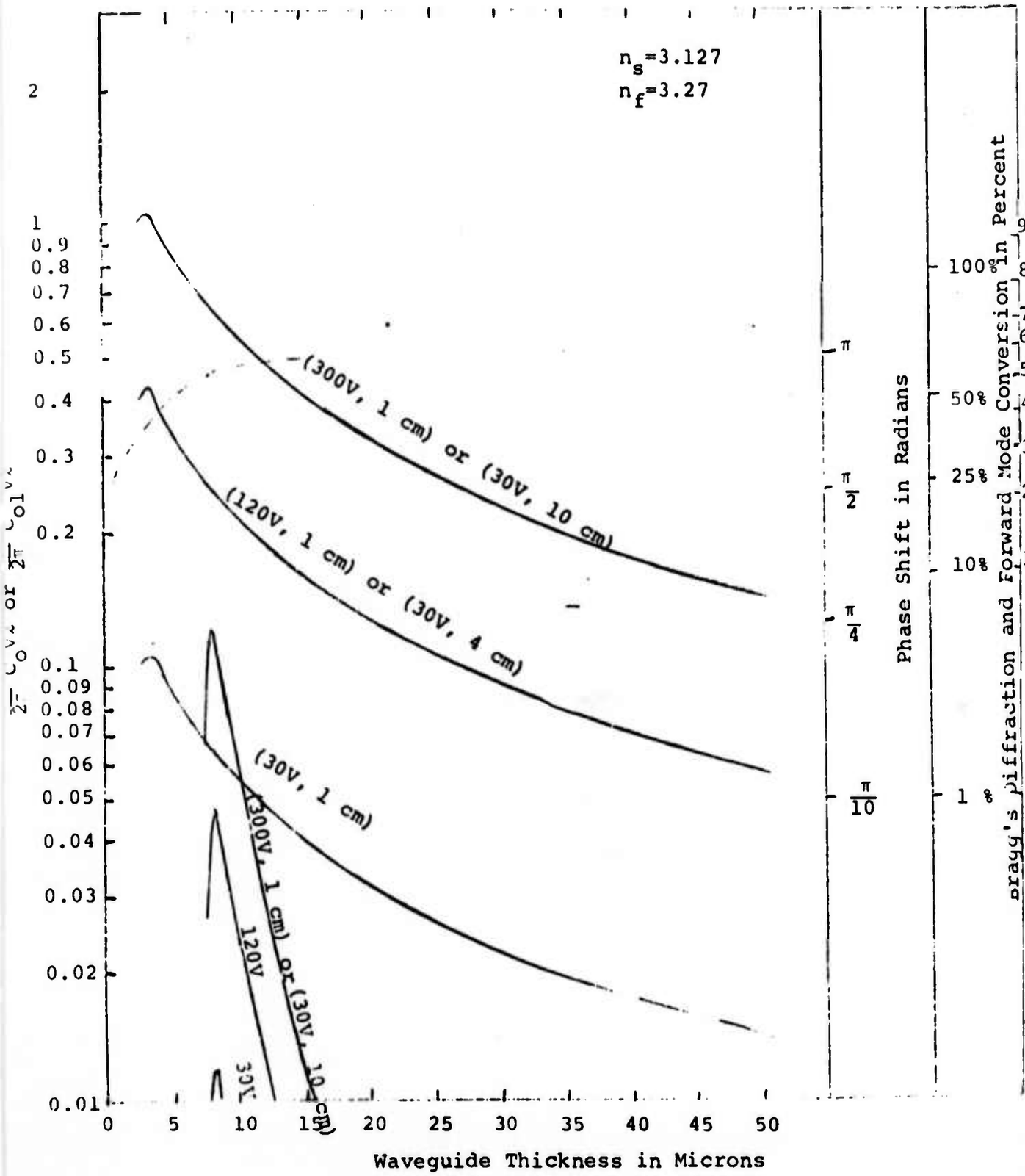

Fig. 5 Modulation Efficiency of Various Modulation Schemes
(n_f = 3.27 n_s = 2.14)

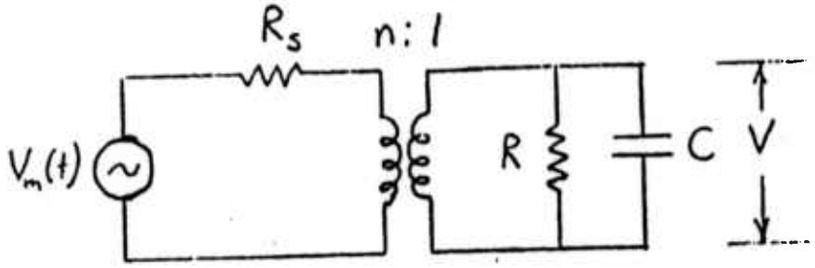

Fig. 6 Equivalent Circuit for Lumped Electro-Optical Modulator

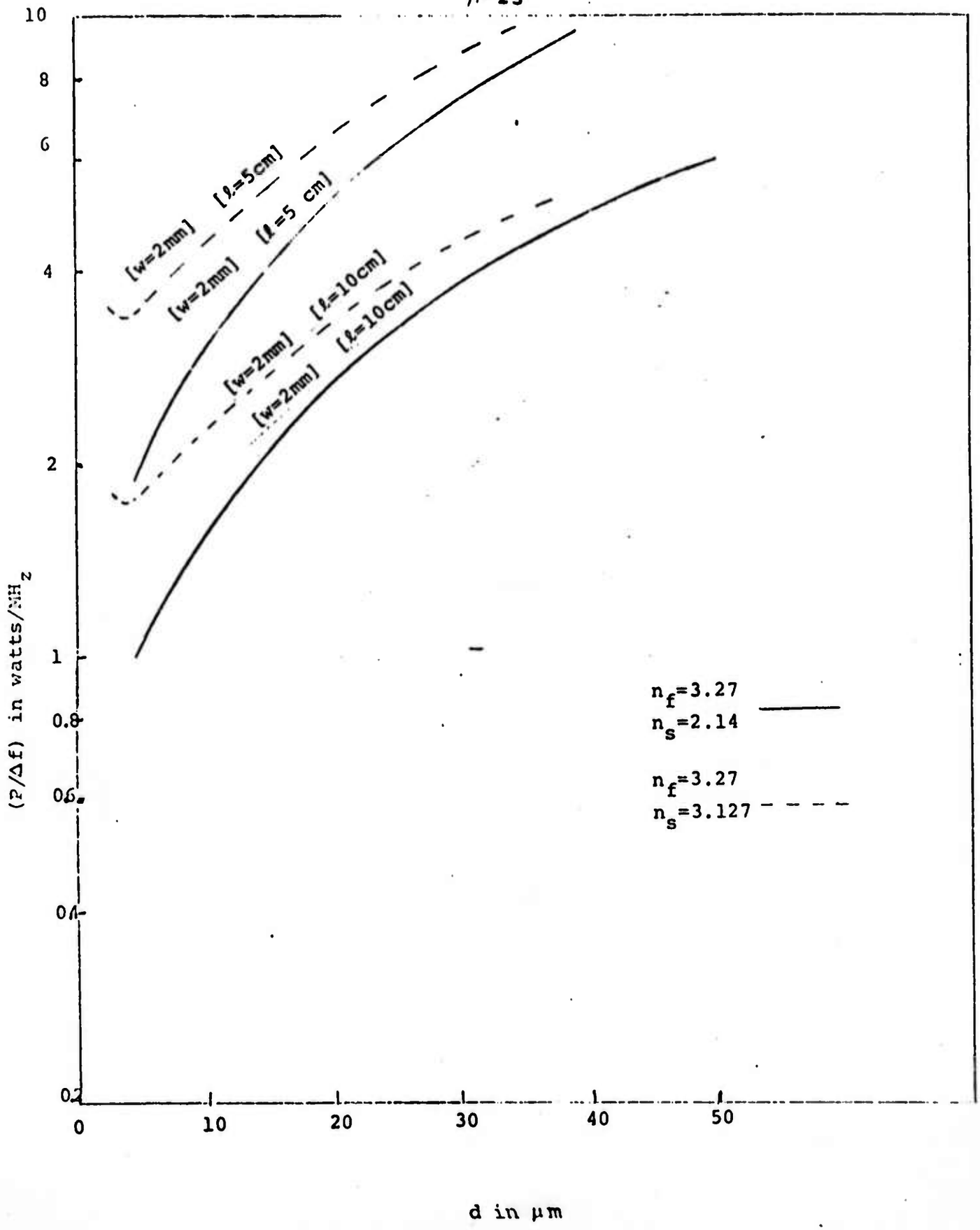

Fig. 7 Power requirement for E-O lumped phase modulator (For Bragg's Modulator and backward wave modulator, multiply P/Δf by $[\pi^2/8 \cos^2\psi]$)

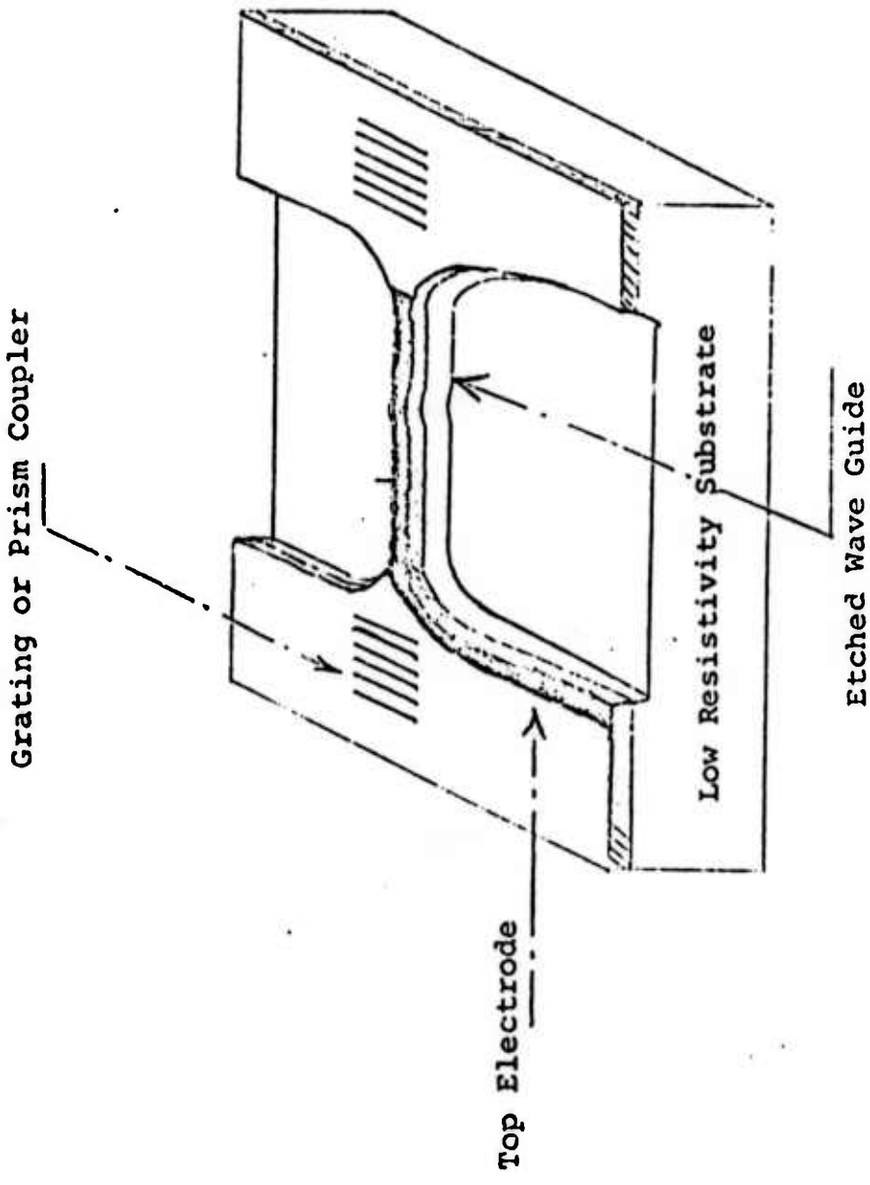

Fig. 8 Two Dimensional Electro-Optical Phase Modulator (amplitude modulation can be obtained when the electrode is made into grating pattern)

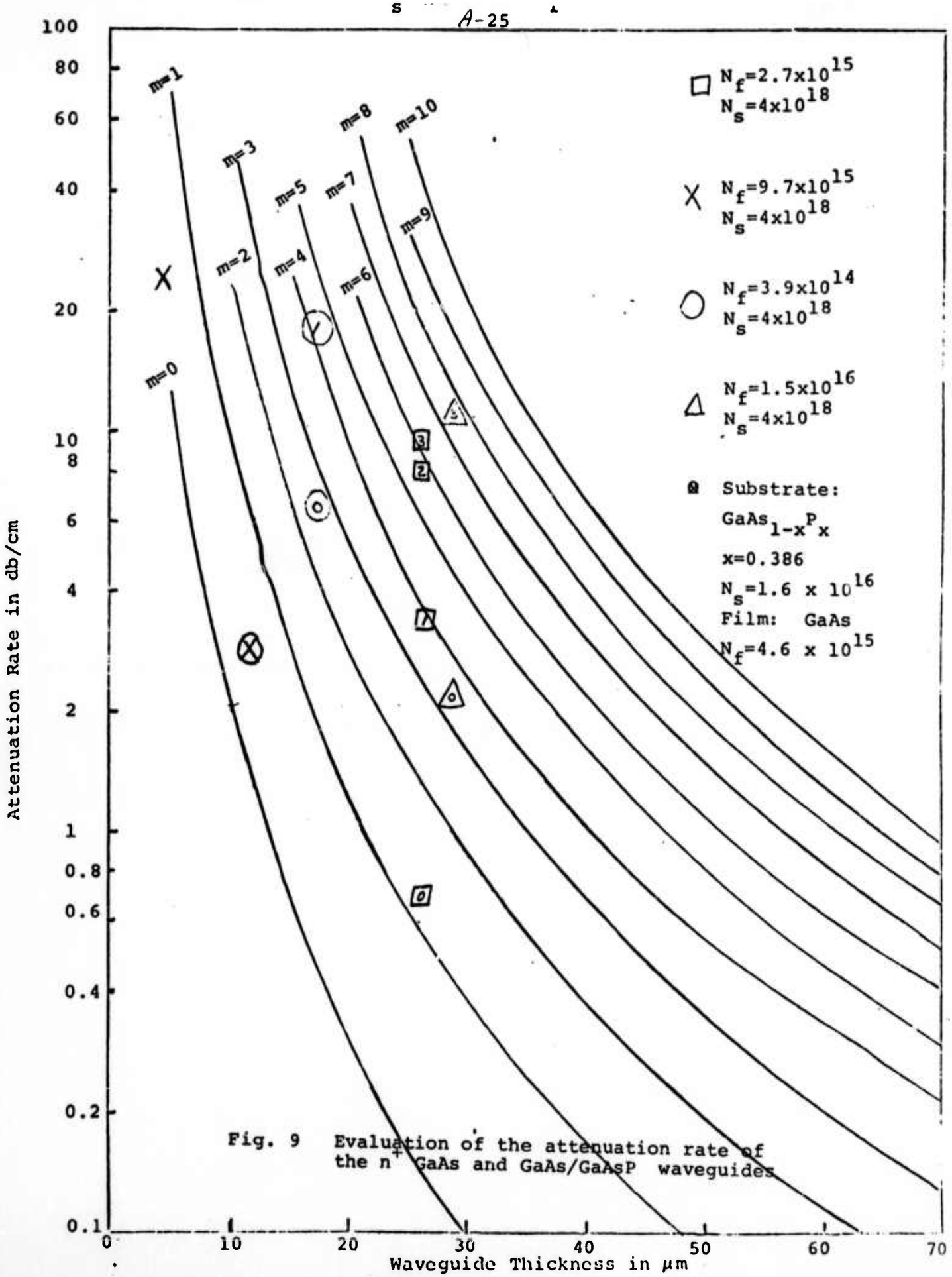

Fig. 9 Evaluation of the attenuation rate of the n^+ GaAs and GaAs/GaAsP waveguides

REFERENCES

1. Kaminow, I. P. and Turner, E. H., Proc. IEEE, 54, 1374 (1966)

2. Kaminow, I. P. and Carruthers, J. R., Appl. Phys. Lett., 22, 326 (1973)

3. Reinhart, F. K. and Miller, B. F., Appl. Phys. Lett., 20, 36 (1972)

4. Other modulation experiments were reported in:

   Hall, D., Yariv, A., and Garmire, E., Optics Communications, 1, 403 (1970)

   Channin, D. J., Appl. Phys. Lett., 19, 128 (1971)

   Cheo, P. K., Appl. Phys. Lett., 22, 241 (1973)

5. Gia, Russo, D. P. and Harris, J. H., Appl. Phys. Lett., 10, 2786 (1971)

6. Polky, J. N. and Harris, J. H., Appl. Phys. Lett., 21, 307 (1972)

7. Ogawa, K., Chang, W. S. C., Sopori, B. L., and Rosenbaum, F. J., IEEE J. Quantum Elect., 9, 29 (1973)

8. Chen, F. S., Proc. IEEE, 58, 1440 (1970)